ASSESSING THE MINERAL AND GEOTHERMAL POTENTIALS OF PART OF KOGI STATE, NIGERIA

BY

KWAGHHUA, Fidelis Iorzua
MTech/SPS/2017/7381

DEPARTMENT OF PHYSICS
SCHOOL OF PHYSICAL SCIENCES
FEDERAL UNIVERSITY OF TECHNOLOGY
MINNA

SEPTEMBER, 2021

ASSESSING THE MINERAL AND GEOTHERMAL POTENTIALS OF PART OF KOGI STATE, NIGERIA

BY

KWAGHHUA, Fidelis Iorzua
MTech/SPS/2017/7381

A THESIS SUBMITTED TO THE POSTGRADUATE SCHOOL, FEDERAL UNIVERSITY OF TECHNOLOGY, MINNA, NIGERIA IN PARTIAL FULFILLMENT OF THE REQUIREMENTS FOR THE AWARD OF THE DEGREE OF MASTER OF TECHNOLOGY IN APPLIED GEOPHYSICS

SEPTEMBER, 2021

ABSTRACT

The Mineral and Geothermal Potentials of part of Kogi State was investigated through the interpretation of aeromagnetic and radiometric data of the study area. Vertical and horizontal derivatives, Analytical Signal, CET, Euler deconvolution and Spectral depth analysis were used for the interpretation of the aeromagnetic data while the Concentration, Ratio and Ternary images of the three radiogenic elements were used for the interpretation of the radiometric data. The analysis of both the Vertical and Horizontal Derivatives revealed features of two major components of Nigerian geology construed in the study area based on the degree of distortion to the magnetic signatures. The NW and SW portion of the area is basement covered by short wavelength magnetic anomalous signatures that are the characteristic of outcrop and shallow intrusive magnetic bodies, while the remaining part of the study area is characterized by medium to long wavelength magnetic signatures that are attributes of sedimentary formations. 1VD map was helpful in delineating mineral potent lineaments. Result of the Analytical Signal amplitude revealed regions with shallow intrusive magnetic rocks having high amplitudes ranging from 0.174 to 0.579 nT/m, while regions with magnetic rock intruding into sedimentary formations at greater depths, have medium to low amplitudes ranging from 0.021 to 0.157 nT/m. Analyses due to Central Exploration Targeting grid revealed lineaments and structures trending NE-SW and E-W. Euler depth analysis revealed structures with greatest depth of 1252 metres and least depth of 27 metres. Radiometric signatures from the K/Th ratio map revealed portions around Latitude 8°00' NW and 7°30' SW having values above known threshold of 0.2 %/ppm for un-altered rocks, to be hydrothermally altered due to K enrichment. Mapping of lithology from Ternary map revealed K-Feldspar mineral bearing rocks dominated the NW and SW regions, while sandstones, ironstones, mudstones, shale, alluvium and other fluvial sedimentary lithologies dominated the sedimentary North-east and South-Eastern regions. Structures trending NE-SW and E-W mapped in the basement region of study area which also coincided with the zones of hydrothermal alterations and thus represents the zones of significant mineralisation in the study area. Result of Spectral depth analysis on the aeromagnetic data showed that peak values of geothermal gradient and Heat flow were 66 °C/km and 166 mW/m^2 respectively, and occurred at the western edge of study area with a Curie point depth of 8 Kilometres.

TABLE OF CONTENTS

LIST OF TABLES

LIST OF FIGURES

CHAPTER ONE

1.0 INTRODUCTION

1.1 Background to the Study

Geophysical investigations of the interior of the Earth involve taking measurements at or near the Earth's surface that are influenced by the internal distribution of physical properties. Analysis of these measurements can reveal how the physical Properties of the Earth's interior vary vertically and laterally (Kearey *et al*., 2002).

Various Geophysical methods for mapping the earth subsurface includes Electrical Resistivity, Induced Polarization, Self-Potential, Electromagnetic, Gravity, Magnetic, Radiometric and Seismic. The application of these methods and their underlying principles has remained the bedrock for mineral exploration and other Geophysical investigations of economic importance. Airborne Geophysical survey makes use of majorly Magnetic, Radiometric and Gravity methods. It is very efficient in mapping out large areas and is cost effective for regional surveys. Airborne geophysical surveys are applicable in oil and mineral exploration, engineering projects, geothermal mapping and land management; they are excellent tools for mapping exposed bedrock, geological structures (such as basements, faults, dikes, sills, kimberlites), sub-surface conductors, paleo-channels, mineral deposits and salinity (Adagunodo *et al.*, 2015).

An aeromagnetic survey is a common type of airborne geophysical survey carried out using a magnetometer on board or towed behind an aircraft. The principle is similar to a magnetic survey carried out with a hand-held magnetometer, but allows much larger areas of the earth's surface to be covered quickly for regional reconnaissance. The aircraft typically flies in a grid like pattern with height and line spacing determining the resolution of the data and cost of the survey per unit area (Allis, 1990).

Aeromagnetic survey is a veritable tool for probing the presence and distribution of magnetic minerals in mineral bearing rocks. Colin (2005) indicated that, the Magnetic properties of any rock are, to some extent, determined by the grain size of the magnetic minerals present.

Radiometric data is collected above the ground by flying an airplane with a spectrometer for regional surveys. The parameter of interest measured during a radiometric survey is gamma radiation which results from the decaying of unstable radioactive elements present in the rocks. Potassium, Uranium and Thorium are the only naturally occurring elements with radioisotopes that produce gamma rays of sufficient energy and intensity to be measured at airborne survey heights (Minty, 1997).

Airborne gamma-ray measurements are a fast way of surveying and monitoring radioactivity of subsurface rocks for the determining of uranium, thorium and potassium concentrations. The radiometric method is one of the most cost-effective and rapid techniques for geochemical mapping based on the distribution of the radioactive elements: potassium, uranium, and thorium. Nowadays, the method is mainly applied for geological mapping and exploration of economic minerals; geochemical and environmental monitoring such as localization of radioactive contamination from fallout of nuclear accidents and plumes from power plants; the method allow the interpretation of regional features over large areas, and is applicable in several fields of science (International Atomic Energy Agency, IAEA, 1990; 2003).

1.1.1 The earth's magnetism

Generally, the Earth is structurally divided into three major components; the Crust, Mantle and Core. The Core is further divided into molten outer-core and solid inner core. Magnetism of the Earth is said to originate from the molten outer core.

Colin (2010) inferred that the movement of the charged electric particles within the molten core produces a magnetic field around the Earth. This magnetic field enveloping the Earth give rise to the magnetic features of the various rocks found within or on the surface of the Earth. The cause of the geomagnetic field is attributed to a dynamo action produced by the circulation of charged particles in coupled convective cells within the outer, fluid, part of the Earth's core (Colin, 2005).

The Earth's magnetic field is made up of three parts namely;

i. The major field, which differs comparatively gradually and originates within the Earth.
ii. The minor field (compared to the major field), which varies rapidly and of external origin.
iii. The spatial variation of the major field which are usually lesser than the major field, are almost the same in time and place, and are brought about by local magnetic anomalies within the Earth's crust. These are the areas of interest in magnetic surveying (Telford *et al*., 1990).

1.1.2 Basic radioactivity

Elements composing of same number of Protons but different number of Neutrons in their atomic structure are called Isotopes. This phenomenon (Isotopy) causes some nuclei to be unstable resulting in spontaneous emission of energetic ionizing radiations to become stable. These isotopes are called radioactive isotopes or radioisotopes. Nuclides with this feature are called radionuclide, and disintegration or nuclear decay is the breakdown of unstable nuclei (International Atomic Energy Agency, IAEA, 2003)

Each radioactive isotope has a distinctive chance associated with the radioactive disintegration of its nuclei. This is called as the isotope half-life and is the time taken for

radioactive nuclei to decay to half its initial value. Hence, after one half-life, half the original radioactive isotopes remain, and after two half-lives, one quarter of the original radioactive isotopes remain (Minty, 1997).

Also, Minty (1997) indicated that radioactivity usually occurs as a sequence of the number of daughter products with a breakdown of the mother elements in order to have a stable isotope. At this period, the behaviours of all the radioisotopes of the decay series are the same. Hence, the extent of the quantity of any daughter nuclei can be helpful in estimating the quantity of any other radio nuclei in the breakdown series. Emanations of gamma rays from the Earth surface differ with many factors but most importantly depend on the amount of radionuclides in the top soil about 30 to 40 cm. The amount depends on the parent rock and the extent of weathering (Elawadi *et al*., 2004).

1.1.3 Mapping natural sources of radiation

Naturally occurring radiation sources can be suitably classified into three groups according to their origin. The first group includes 40K, 238U, 235U and 232Th, which are believed to have been produced during the creation of the universe and have half-lives of the same order as the Earth's age. The second group comprises radioactive isotopes that are daughter products from the decay of isotopes in the first group. These have half-lives varying from small fraction of one 1 second to 10^4 to 10^5 years. The third group include isotopes created by external causes such as the reactions of cosmic radiations with the Earth and its atmosphere. The concentration of cosmic radiation at surface of Earth is comparatively small such that all of them are absorbed in the atmosphere (Minty, 1997).

1.1.4 Geothermal energy

Geothermal energy is the heat produced deep in the Earth's core. It is a clean, renewable resource that can be harnessed for generation of electricity and other industrial heating requirements. The vast majority of Earth’s heat is constantly generated by the decay of radioactive isotopes, such as potassium, thorium and Uranium. As earth’s temperature rises with depth from the surface to the core, the gradual change in temperature is known as the Geothermal Gradient. Measurements have shown that a region with significant geothermal energy is characterised by an anomalous high temperature gradient and heat flow (Tselentis *et al*., 1991). The depth to bottom of magnetic sources (DBMS) or curie point depth (CPD) is known as the depth at which the dominant magnetic mineral in the crust passes from a ferromagnetic state to a paramagnetic state under the effect of increasing temperature(where magnetisation is lost) (Nagata, 1961). It is therefore expected that geothermally active areas would be associated with shallow Curie point depth (Nuri *et al*., 2005).

1.2 Statement of the Research Problem

One of the major problem bedevilling the country against benefiting immensely from its abundant solid mineral and other sub-crustal resources is the size of the country. With a land mass totalling about 923,768 Square Kilometres, exploration for solid mineral and appropriation of other natural resources such as geothermal energy could remain elusive until a comprehensive geophysical exploration is carried out that will delineate these resources locations in coordinate and depth. The availability of such a database will become a tool that will attract investors who are interested in mineral exploration and utilization of geothermal energy for electricity generation and other industrial processes.

This will not only solve electrification problem but also increase the revenue accrued to the nation, as well as help in diversifying the revenue base from crude oil to other sources.

1.3 Aim and Objectives of the Study

The aim of this research is to interpret the Aeromagnetic and Radiometric data of part of the confluence area in order to assess the mineral and geothermal potentials associated with it.

The objectives of the research include the following:

i. Delineate structures, lineaments and depth to magnetic sources from Vertical derivatives, Horizontal derivatives Analytical Signal, Centre for Exploration Targeting (CET) and Euler deconvolution.
ii. Compute Concentration maps, and use the result to produce Ratio and Ternary images to map lithologies and locate regions of Hydrothermal Alterations.
iii. Correlate the delineated structures with mapped lithologies and regions of hydrothermal alterations to map zones of mineralisation.
iv. Employ spectral analysis technique on the aeromagnetic data to reveal underlying geothermal potentials of study area.

1.4 Justification of the Study

Nigeria is one of the Nations colossally blessed with solid minerals and other sub-crustal resources such as geothermal energy. Employing these resources will not only enhance her infrastructural development but will also boost her economic and revenue base. This research work will produce database of Geophysical information for the exact location (Coordinates and depth) of solid minerals and geothermal potential of study area. These information makes mineral exploration easier and will attract investors whose input will increase Internally Generated Revenue (IGR) of the country.

CHAPTER TWO

2.0 LITERATURE REVIEW

2.1 Geology of Kogi State

The geological setting of Kogi State is unique in view of the occurrence of the two major components of Nigerian geology (Basement Complex and Sedimentary Basin). Approximately, half of the State is covered by crystalline Basement Complex while the other half is covered by Cretaceous to Recent sediments.

The Basement Complex are predominantly underlain the western flank of the State. They are made up of Migmatite-Gneiss Complex which include rocks of migmatites, gneisses and granite-gneisses; the Schist Belts (metasedimentary and metavolcanic rocks) which include phylites, schists, pelites, quartzites, marbles and amphibolites; and the Pan-African Older Granites consisting of granites, granodiorites, syenites, monzonites, gabbro and charnockites. The crystalline complex contained economic minerals such as iron ore, gemstones, quartz, feldspar and other associated minerals, while the Pan-African Older Granite contained cassiterite, tantalite, columbite, gemstones and other associated minerals (Kogi State Ministry of Solid Minerals Development, KSMSMD, 2004)

The geological setting of the study area which is an extraction from the geology of kogi state can be seen in Figure 2.1.

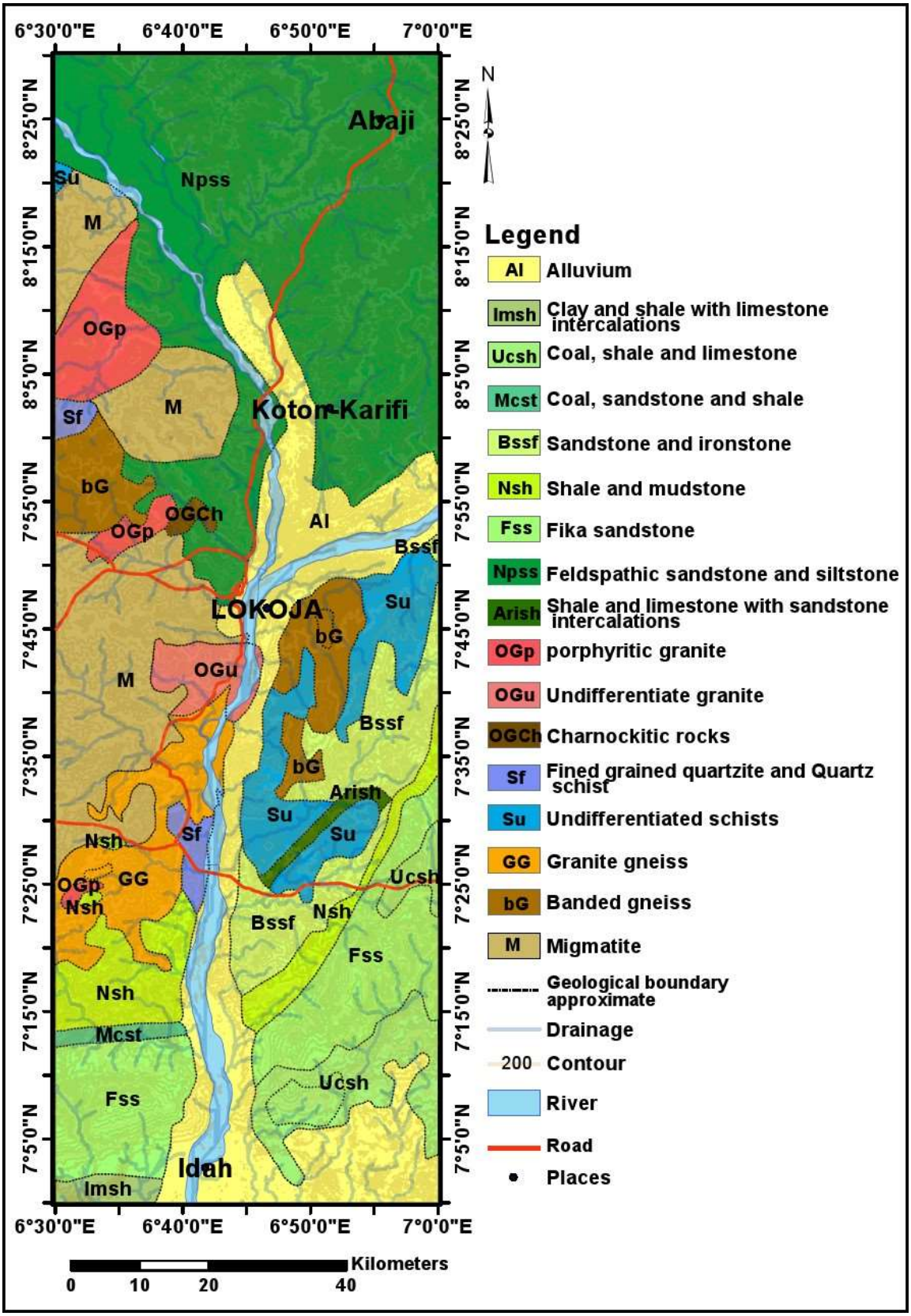

Figure 2.1 Geological map of study area (Adapted from geological map of Nigeria, NGSA 2009)

2.2.1 Mineralization

Magneto-metric surveys can be useful in defining magnetic anomalies which represent ore (direct detection), or in some cases gangue minerals associated with ore deposits (indirect or inferential detection). The most direct method of detection of ore via magnetism involves detecting iron ore mineralisation via mapping magnetic anomalies associated with banded iron formations which usually contain magnetite in some proportion. Skarn mineralisation, which often contains magnetite, can also be detected though the ore minerals themselves would be non-magnetic. Similarly, magnetite, hematite and often pyrrhotite are common minerals associated with hydrothermal alteration, and this alteration can be detected to provide an inference that some mineralising hydrothermal event has affected the rocks (Adagunodo *et al.,* 2015).

2.2.2 Iron ore and associated mineral resources of study area

The banded iron formation of Nigeria generally occurs in metamorphosed folded bands, associated with Precambrian basement complex rocks which include low grade metasediments, high grade schist, gneisses and migmatites. Included in these group are the well-known Lokoja Okene District occurrences notably at Itakpe, Ajabanoko, Kakun, Chokochoko, Toto Muro and Tajimi. In the north western parts of Nigeria, the banded iron formation occurs sporadically in narrow bands and lenses interbedded with pelitic and semi pelitic phyllites and schists. Three main facies of these bands have been identified as the oxide, silicate and sulphide facies. The Cretaceous sedimentary iron formation described as sedimentary are partly lateritic in character. Two of such deposits include the oolitic iron stones of the Agbaja Plateau and the rubbly iron stone of Enugu. Similar iron stones have been found as caps of varying dimensions on some Cretaceous successions of the Illumeden and Niger embayment notably around Koton karfe and Bida basin. (Ministry of Mines and Steel Development, MMSD, 2010)

Feldspar and Granite: Feldspar is an alumina silicate mineral containing varying proportions of calcium, sodium, potassium, and other elements. Feldspars are essential constituents of most igneous rocks; they frequently occur in metamorphic rocks and in many sedimentary rocks. The type of feldspar most common in Kogi State is potassium-rich feldspar (K-feldspar). Granite is a coarse-grained igneous rock composed of feldspar (usually potash feldspar and oligoclase) and quartz with a small amount of mica (biotite and muscovite). Large deposits of feldspar and granite are found all over the western flanks of the State.

Magnetite: Magnetite is iron oxide, Fe_3O_4 black and strongly magnetic mineral. It is an ore of iron, although it can be found in the form of octahedral steel-black crystals with a metallic luster, it occurs more commonly as compact and granular masses. Magnetite is a major source of iron. Magnetite is found at Agbaja Plateau, Tajimi Ridge and Patti Ridge in Lokoja LGA; Gboloko in Bassa LGA; Akpogu in Mopa Muro LGA; and Ebiya in Ajaokuta LGA.

Marble: Marble is a fine- to coarse-grained metamorphic rock consisting mainly of recrystallized calcite ($CaCO_3$) and/or dolomite ($CaMg(CO_3)2$). It is a metamorphosed limestone. Marble deposits in the State are localized within the highly metamorphosed metasediments of the Basement Complex. Large proved reserves of marble deposits occur mostly in the western flank of Kogi State

2.3 Review of Relevant Literatures

Olasheinde *et al*. (2012) interpreted Aeromagnetic anomaly map of Koton-Karfi (Sheet 227) which was profiled into 5 equal sections (North-South) for depth to base estimation employing Poorna C. Pal's mathematical modelling method. The anomaly map was sectioned into nine equal squares for brief spectral qualitative description. From the

profiles it was observed that, depth-to-basement thickness of the sediments ranges between 600m and 1,100m increasing from south to north of the sheet.

Adetona and Mallam (2013) estimated the thickness of sedimentation within lower Benue Basin and Upper Anambra Basin, Nigeria, Using both spectral depth determination and source parameter imaging. Spectral depth analysis result showed that a maximum depth above 7 km was obtained within the cretaceous sediments of Idah, Ankpa, and below Udegi at the middle of the study area. Minimum depth estimates between 188.0 and 452meters were observed around the basement regions. Results from source parameter imaging shows a minimum depth of 76.983 meters and a maximum thickness of sedimentation of 9.847 km, which also occur within Idah, Ankpa, and Udegi axis.

Adetona and Mallam (2013) investigated the structures within the Lower Benue and Upper Anambra basins, Nigeria. The aeromagnetic data over the study area was subjected to both Vertical and Horizontal Derivatives, Analytical Signal and CET grid analysis. Results from the Vertical and Horizontal derivatives showed short wavelength magnetic signatures at the Northern and Western edge of the area, while the remaining part of the area is characterized by medium to long wavelength magnetic signatures which are indicatives of shallow intrusive bodies and thick sedimentations respectively. The Analytical Signal reveals regions with outcrop of magnetic rocks having amplitudes ranging from 0.230 to 0.40, areas with magnetic rock intruding into sedimentary formations at shallow depths, with amplitudes ranging from 0.094 to 0.229 cycles, while regions with magnetic rock intruding into sedimentary formations at greater depths, having very low amplitudes ranging from -0.085 to 0.055 cycles. Analyses due to CET grid analysis equally reveal the basement rocks to the North and Southern edge of the study area.

Salako (2014) carried out depth to basement determination using source parameter imaging (SPI) of aeromagnetic data: An application to upper Benue trough and Borno basin, northeast, Nigeria. The result of the source parameter imaging (SPI) has its highest sedimentary thickness of about 5.0km around Gombe, AkoGombe, Bulkachuwa and Damaturu areas. The shallow sedimentary thickness could also be found in basement complex around Bauchi, Kaltungo inlier and volcanic areas at the eastern part of the study area.

Chinwuko *et al*. (2014) interpreted Aeromagnetic data over Lokoja and environs qualitatively and quantitatively using the slope method. Results supported by geological information revealed two depth sources in the study area; on the average the deeper magnetic sources range from 2.3 to 4.9 km, while the shallower magnetic sources range from 1.1 to 1.6 km. Visual study of the residual anomaly map showed the presence of igneous intrusive in the entire North and Southwestern part of the study area. The First Vertical Derivative (1VD) lineament map showed Faults trending in Northwest-Southwest (NW-SW) and Northeast-Southwest (NE-SW) direction and this conforms to the Niger-Benue basin itself.

Akanbi *et al.* (2015) estimated the regional magnetic field trend and depth to magnetic rocks within Maijuju area, North-Central, Nigeria. The TMI map revealed anomalies observed in the study area to trend largely in the NE-SW and EW directions. Low magnetic intensities values were observed at Jos-Bukuru, Jarawa, Shere, and Kofai and Rop Complexes. Intermediate negative magnetic values (-54.5 to -5.3 nT/m) were observed at the Sara-Fier Complex. Positive magnetic intensity range of 72.9 to 270.7nT/m was seen to dominate the Older Granite region, the Basement Complex and part of Sara-Fier Complex.

Obiora *et al*. (2016) interpreted the Aeromagnetic data of Idah area (sheet 267), north-central Nigeria, by applying Euler deconvolution. Computing Euler deconvolution for various structural indices (SI), the depth obtained for SI=1, ranges from 5.6m to 197.6m, 22.0m to 204.7m for SI=2 and for SI=3, the depth to magnetic source obtained ranges from 38.0m to 205.5m.

Nwankwo and Abayomi (2017) estimated the Curie-point depths, succeeding geothermal gradients and subsurface crustal heat flow from the spectral centroid analysis of the high resolution Aeromagnetic data of the entire Bida Basin in north-central Nigeria. The result showed that the CPD varied between 15.57 and 29.62 kilometres with an average of 21.65 kilometres, the geothermal gradient varies between 19.58 and 37.25 °C /km with an average of 27.25 °C/km, and the crustal heat flow varied between 48.41 and 93.12mWm^2 with an average of 68.80mWm^2.

Fatoye (2018) carried out an extensive study on the Geology and mineral resources of Kogi state and inferred that The geological setting of Kogi State comprises two major components of Nigerian geology (Basement Complex and Sedimentary Basin). The Basement Complex is made up of Migmatite-Gneiss Complex, the Schist Belts and the Older Granites and the sedimentary area, which is the Anambra and Bida Basin, consists of sedimentary rocks that form part of Cretaceous to Recent sediments of Nigeria.

Nwobodo *et al*. (2018) Interpreted high resolution Aeromagnetic data covering Lokoja and Dekina. Forward and Inverse modelling techniques were employed in quantitative interpretation. The result from the forward and inverse modelling analysis of airborne magnetic data showed that susceptibility values obtained from the modelled profiles 1 - 5 are 0.0003,0.0002,0.025,0.040,0.0009 SI respectively, with respective depths of 2607, 2911, 1477, 1627 and 1874 m. The modelling of the residual map revealed some minerals

in the study area, which are; Casseterite, Clay and rock bearing minerals like Granite, limestone, Dolomite and marble.

Akinnubi and Adetona (2018) estimated the geothermal potential within the eastern part of Lower Benue Basin using spectral depth analysis from Aeromagnetic data and correlating the results with the analysis of radiometric concentration data of the study area. Results showed that Curie Point Depth varied between 9 to 18 kilometres, Heat flow varied between 76 to 135 mW/m2 and the geothermal gradient varied between 30 °C/km to 54 °C/km.

Adewumi *et al*. (2019) estimated geothermal parameters over part of Bida basin using aeromagnetic data. Spectral analysis yielded depth to top of basement ranges from 1.59 km to 6.38 km. The CPD range from 10.88 km to 35.51 km with an average value of 23.22km. The geothermal gradients range from 16.33 °C/km at the centre of the southern region of the area to 53.30 °C/km at the north-eastern and north western region of the study area with an average of 28.98 °C/km. While the heat flow range from 40.99 mW/m^2 to 133.80 mW/m^2 with an average value of 76.19 mW/m^2. The South-eastern, southwestern, and the north-western part of the study area might be a good indicator of geothermal energy potential.

Ibe and Nwokeabia (2020) applied air-born radiometric method in geologic mapping of Malufashi area and Environs, North-western Nigeria. The abundance ratios, U/Th, U/K and Th/K and the ternary images of the three radioactive elements were produced. The images obtained from the radiometric data showed that the study area comprises five major rock types, based on their variation in the concentration of the three radioactive elements. Hydrothermal alteration zones were mapped. The altered zones were noted to be associated with mineralization in the quartzite rich schist formation.

CHAPTER THREE

3.0 MATERIALS AND METHODS

3.1 Location of Study Area

The study area is part of the confluence region denoting the region where river Benue and river Niger coincide. It is situated at the left and right hand side of the river Niger cutting across Koton-Karfi, Lokoja down to Idah. It is bounded by Latitude 7.0°N to 8.5°N and Longitude 6.5°E to 7.0°E. The study area projected from Administrative map of Nigeria is shown in Figure 3.1.

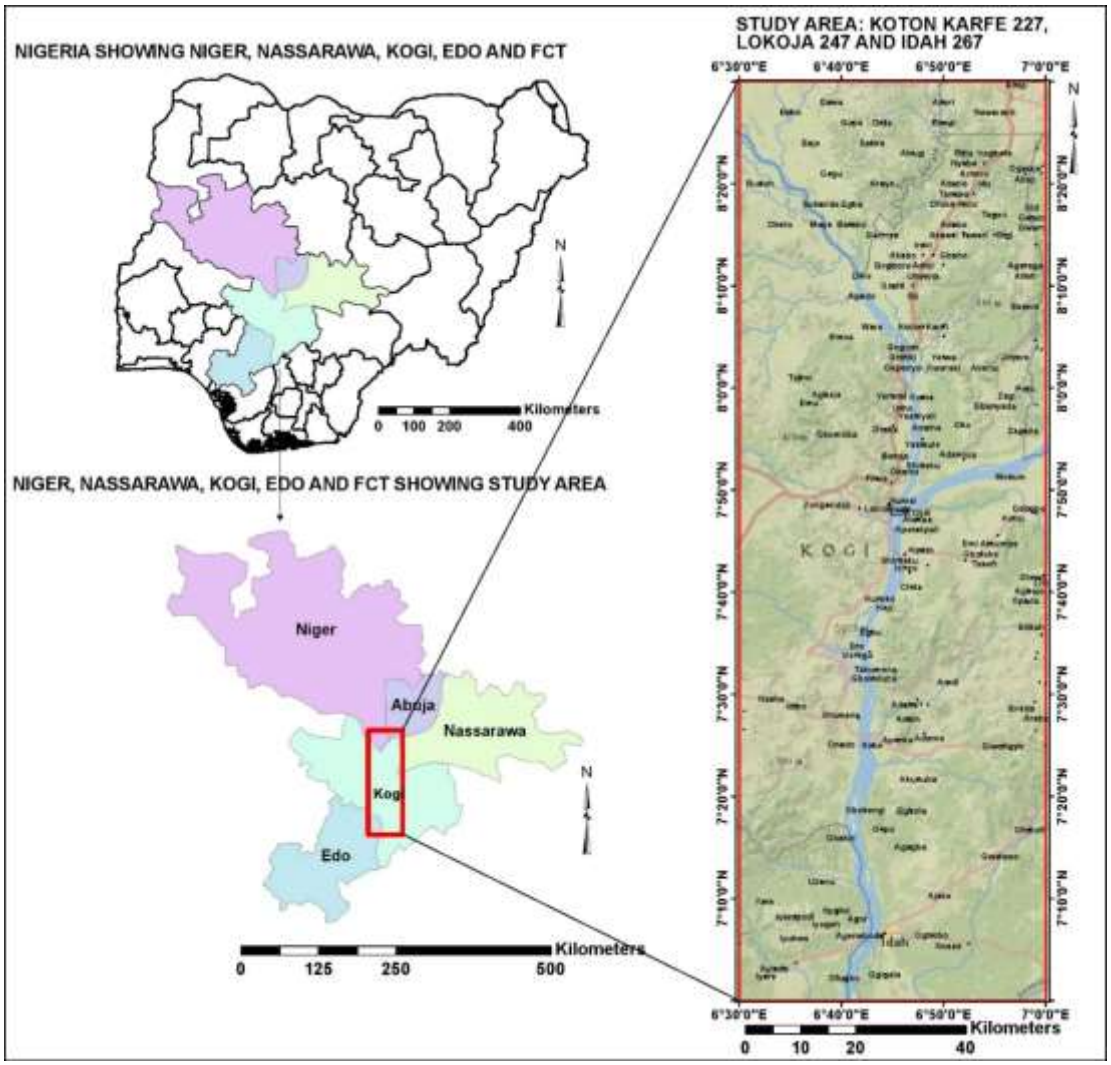

Figure 3.1 Location of study area projected from administrative map of Nigeria.

3.1.1 Data source

The Aeromagnetic and radiometric data that was used for this research work was obtained from the Nigeria Geological Survey Agency (NGSA). The NGSA is a parastatal under the Ministry of Mines and Steel Development saddled with the statutory role of providing up-to-date Geoscience information related to rocks, minerals and groundwater resources of Nigeria. The details of data specifications is shown in the Table 3.1 below:

Table 3.1 Survey data parameter and specifications (NGSA, 2009)

Survey Parameter	**Parameter Specification**
Data Acquired by:	Fugro Airborne Surveys
Time Range	2005 – 2009
Magnetic data Recording Interval	0.1 seconds or less
Sensor Mean Terrain Clearance	80 meters
Flight Line Spacing	500 meters
Tie Line Spacing	5000 meters
Flight Line trend	135 degrees
Tie Line trend	45 degrees
Equipment: Aircraft	Cessna Caravan 208B ZS-FSA, Cessna Caravan 208 ZS-MSJ,
Equipment: Magnetometer	3 x Scintrex CS3 Cesium Vapour

3.2 Method

Series of filters were applied to the Aeromagnetic and radiometric data in order to reveal features that will aid in the interpretation of the data. The mathematical algorithm and enhancement techniques applied includes:

i. Computation and reduction of the Aeromagnetic data to equator and pole to remove the effect of Inclination and Declination angle.
ii. Computation of Vertical and Horizontal derivative to enhance near surface structures and subdue regional structures.

iii. Computation of Analytical Signal to map the edges of the permanently magnetized sources and centralize anomalies over their causative bodies in areas of low magnetic latitude.

iv. Computation of Centre for Exploration Targeting (CET) to delineate deep lineaments.

v. Application of Euler deconvolution tool to determine the location and depth of causative bodies.

vi. Computation of concentration maps for Uranium, Thorium and Potassium to delineate regions of high and low concentration of radioactive elements.

vii. Computation of Potassium Composite map by combining Potassium (K) in ratio (K/Th) and (K/U) to determine variation in concentration of potassium.

viii. Computation of Uranium Composite map by combining Uranium (U) in ratio of (U/Th) and (U/K) to determine variation in concentration of Uranium.

ix. Computation of Thorium Composite map by combining Thorium (Th) in ratio of (Th/U) and (Th/K) to determine variation in concentration of Thorium.

x. Computation of Ternary maps by combining data of Potassium (K), Thorium (Th) and Uranium (U) to map lithology

xi. Compute spectral analysis to estimate Curie point depth, Heat flow and Geothermal gradients.

3.3 Aeromagnetic data processing

A range of imaging routines can be specified to visually enhance the effects of selected geologic sources using mathematical enhancement techniques (Milligan and Gunn, 1997). The images were produced in the Geosoft® software package (Oasis Montaj), and exported in the JPEG format. To investigate the structures that could be host to solid minerals such as Gold, Marble, Gemstones, Chromium, Clay, kaolin and Iron Ore in the

area, a combination of filters and algorithms were employed among which are Total magnetic Intensity map reduced to Equator and Pole, First Vertical Derivative, Horizontal derivatives (DX, DY and DZ), Analytical Signal, CET and Euler Deconvolution. Results from these operators yielded a set of resolution that gives adequate interpretations.

3.3.1 Reduction to the pole

Shape of a magnetic total intensity anomaly is affected by the directions (inclination and declination) of the magnetization and the earth's magnetic field vectors. The process of reduction to the pole is commonly used to remove this effect of inclination and declination and to centre the anomaly over the causative body. RTP also helps in the interpretation of magnetic data by removing the influence of magnetic latitude on the anomalies. (Lu *et al*., 2003)

Reduction to the Pole is given as (Gosoft, 2010):

$$L(\Theta) = \frac{1}{(\sin(la)+i\cos(l).\cos(D-\Theta)^{2}} \qquad (3.1)$$

where:

l = Geomagnetic inclination

la = Inclination for amplitude correction

D = Geomagnetic declination

3.3.2 Reduction to equator

It is a filtering process that recomputes the magnetic total intensity anomalies as if the causative bodies were magnetized in a horizontal direction. Anomalous lows would then be centred over the bodies after filtering. For the convenience of interpretation, a 180-degree phase reversal is introduced so that troughs become peaks, still positioned over the centres of the bodies. The reduction-to-the-pole filter is stable only at high magnetic

latitudes but the reduction-to-the-equator filter is well behaved in low and high magnetic latitudes (Li, 2008)

Reduction to Equator is given by the formula:

$$L(\theta) = \frac{[\sin(I) - i.\cos(I).\cos(D-\theta)]^2 X \left(-\cos^2(D-\theta)\right)}{\left[\sin^2(I_a) + \cos^2(I_a).\cos^2(D-\theta)\right] X \left[\sin^2(I) + \cos^2(I).\cos^2(D-\theta)\right]}, if\ (|I_a|) < (|I|), I_a = I \quad (3.2)$$

where

I = geomagnetic inclination

Ia = inclination for amplitude correction

D = geomagnetic declination

Sin (I) is the amplitude component while icos(I)cos(D-θ) is the phase component

3.3.3 First vertical derivative filter

The application of the vertical derivative filter to a magnetic data is to improve the shallowest magnetic features and suppress the deeper anomalies in the data (Geosoft Inc, 1996). The filter attempts to attenuate the long wavelength regional features within a potential data and in the same vein accentuate the shallow features that are high in frequency of occurrence. The function can be mathematically related as:

$$L(r) = r^n \quad (3.3)$$

where n depict the order of differentiation generally 1 or 2, r signifies the wave number in radians per ground unit and L is cycle/ground unit in which the survey was conducted e.g. metres, feet, Kilometre etc.

3.3.4 Horizontal derivative (DX, DY, DZ)

The Horizontal derivative tends to sharpen the edge of anomalies and enhance shallow features. The resultant map is much more responsive to local influence than to broad or regional deep seated anomalies.

If T is the total magnetic field and x and y represent two orthogonal horizontal directions, then the magnitude of the Horizontal gradient HGM as given by (Cordell and Grauch, 1985) is:

$$\text{HGM} = \sqrt{\left(\frac{\partial T}{\partial X}\right)^2 + \left(\frac{\partial T}{\partial Y}\right)^2} \quad (3.4)$$

Total horizontal derivative is a good edge detector because it computes the maxima over the edges of the structures. The horizontal gradient method measures the rate of change in magnetic susceptibility in the ***x*** and ***y*** directions and produces a resultant grid. The gradients are all positive making this derivative easy to map.

3.3.5 Analytical signal amplitude

The analytical method gives the amplitude response of an anomaly. This filter applied to magnetic data is aimed at simplifying the fact that magnetic bodies usually have positive and negative peak associated with it, which may make it difficult to determine the exact location of causative body. For two dimensional bodies a bell shaped symmetrical function is derived and for a three dimensional bodies the function is amplified of analytical signal. This function and it derivatives are independent of strike, dip, magnetic declination, inclination and remanent magnetization (Debeglia and Corpel 1997)

The analytic signal is a function related to magnetic fields by the derivatives:

$$\text{AS} = \sqrt{\left(\frac{\partial A}{\partial X}\right)^2 + \left(\frac{\partial A}{\partial Y}\right)^2 + \left(\frac{\partial A}{\partial Z}\right)^2} \quad (3.5)$$

This function is extremely interesting in the context of interpretation, in that it is completely independent of the direction of the magnetization and the Earth's magnetic field. The interpretation of analytic signal maps and images in principle, provides simple and easily understandable indications of magnetic source geometry, the half widths of these peaks can be linearly related to depths, if the sources of the peaks are vertical magnetic contacts (Roest and Pilkongton, 1992).

3.3.6 CET (Centre for exploration targeting)

The CET Grid Analysis tool is useful for texture and phase analysis, also structure, lineament, edge, and threshold detection. The extension as used in Oasis Montaj Software is specifically enhanced for mineral exploration geoscientists probing for discontinuities within magnetic data. The CET Grid Analysis provides a step-by-step trend detection menu which offers two different approaches to trend estimation. The first method, Texture analysis-based image enhancement, is suitable for analysing regions of subdued magnetic responses where texture analysis can first enhance the local data contrast. The second method, Discontinuity structure detection, is useful in identifying linear discontinuities and edge detection (Geosoft., 2010)

3.3.7 Euler deconvolution

The objective of the Euler deconvolution process is to produce a map showing the locations and the corresponding depth estimations of geologic sources of magnetic anomalies in a two-dimensional grid (Reid *et al*., 1990).

Thompson (1982) showed that Euler's homogeneity relation could be written in the form

$$(x - x_0)\frac{\delta T}{\delta X} + (y - y_0)\frac{\delta T}{\delta Y} + (z - z_0)\frac{\delta T}{\delta Z} = N(B - T) \quad (3.6)$$

where (x_0, y_0, z_0) is the position of a magnetic source whose total field T is detected at $(x, y, z,)$. the total field has a regional value of B. The degree of homogeneity N may be

interpreted as a structural index (SI) (Thompson, 1982), which is a measure of the rate of change with distance of a field.

3.4 Radiometric data processing

Procession and analysis of radiometric data set is done with the major aim of identifying radiometric signatures associated with the host rocks relevant to mineralization. It is a major tool for mapping the lithology of an area under investigation. The spatial correlation of the radiometric data involves measuring of naturally occurring radioactive elements that exist in minerals forming rock and soil (Telford *et al*., 1990). High radiometric elemental patterns and irregular low magnetic zones are interpreted to have resulted from possible mineral deposits or rock alterations (Gunn *et al*., 1997).

3.4.1 Concentration mapping of Potassium (K), Thorium (Th) and Uranium (U)

Oasis Montaj Geosoft software was used to generate the total count images through mini-curvature gridding tool. The images were correlated with geological units, patterns and trends which showed regions of strong potassium, uranium and thorium concentration.

Potassium is a major constituent of many rock types and comprises about 2% of the Earth's crust. In contrast, Uranium and Thorium are minor constituents of the Earth's crust and average 2.5 ppm (or mg/kg) and 9 ppm, respectively (Gunn *et al*., 1997). Potassium-bearing minerals include feldspars and micas. Thorium which is usually considered immobile is typically found in allanite, monazite, xenotime, and zircon. Uranium occurs in U-oxide and in U-silicate minerals.

3.4.2 Ratio maps and ternary images

In order to get rid of lithological differences and variations caused due to soil moisture, nonplanar nature of the host rock and errors related with altitude correction, ratio images were produced. Silva *et al*. (2003) inferred that lithological variations have a tendency to

be removed because radioelement amounts normally change as lithology change. A combination of Potassium, Thorium and Uranium concentration maps was used to generate Ternary.

3.5 Curie Point Depth, Heat Flow and Geothermal Gradient

The Aeromagnetic data was subjected to spectral depth analysis in order to access the geothermal parameters (Curie Point Depth, Heat Flow and Geothermal Gradient).

Bhattacharyya and Leu (1975, 1977) introduced the mathematical models of the centroid method based on the examination of the shape of isolated magnetic anomalies and the study of the statistical properties of magnetic ensembles by Spector and Grant (1970). Blakely (1995) subsequently introduced power spectral density of total magnetic field, $\phi\Delta T(k_x, k_y)$ as

$$\phi\Delta T(k_x, k_y) = \phi_M(k_x, k_y).4\pi^2 {C_M}^2 |\Theta_M|^2 |\Theta_f|^2 e^{-2|k|Z_t}\left(1 - e^{-2|k|(Z_b - Z_t)}\right)^2 \quad (3.7)$$

where k_x and k_y are wave numbers in x and y direction, $\phi_M(k_x, k_y)$ is the power spectra of the magnetization, C_M is a constant, Θ_M and Θ_f are factors for magnetization direction and geomagnetic field direction, and Z_b and Z_t are depths to bottom and top of magnetic layer respectively.

If the layer's magnetization, $M(x, y)$ is a random function of x, y it implies that $\phi_M(k_x, k_y)$ is a constant, and therefore the azimuthally averaged power spectrum, $\phi(|k|)$ would be given as

$\phi(|k|) = Ae^{-2|k|Z_t}\left(1 - e^{-2|k|(Z_b - Z_t)}\right)^2$ The depth to the top of the magnetic source is therefore derived from the slope of the high-wave-number portion of the power spectrum as:

$$\ln\left(P\left((k)^{\frac{1}{2}}\right) = A - |k|\mathrm{Z_t}\right. \quad (3.8)$$

where $P(k)$ is the azimuthally averaged power spectrum, k is the wave number $(2\boldsymbol{\pi}\ \boldsymbol{k}m^{-1})$, A is a constant, and Z_t is the depth to the top of magnetic sources.

The centroid depth of magnetic sources can also be calculated from the low-wave-number portion of the wavenumber- scaled power spectrum as (Tanaka *et al*., 1999)

$$\ln(P\left((k)^{\frac{1}{2}}/k\right) = B - |k|\mathrm{Z}_0 \qquad (3.9)$$

where B is a constant and Zo is the centroid depth of magnetic sources.

The depth to the bottom of the magnetic source (Z_b) can subsequently be obtained from the relation (Okubo *et al.*,1985)

$$Z_b = 2Z_0 - Z_t \qquad (3.10)$$

Using the depth to the bottom of magnetic sources (Z_b), the geothermal gradient $\left(\frac{dT}{dZ}\right)$can be estimated as (Tanaka *et al*., 1999; Ross *et al*., 2006)

$$\left(\frac{dT}{dZ}\right) = \left(\frac{\Theta_c}{Z_b}\right),$$

where Θ_c is the Curie temperature.

Next, using Z_b and $\frac{dT}{dZ}$, the heat flow (q_z) can similarly be estimated as (Okubo *et al*., 1985)

$$q_z = -\sigma\left(\frac{\Theta_c}{Z_b}\right) = -\sigma\left(\frac{dT}{dZ}\right), \qquad (3.11)$$

where σ is thermal Conductivity. Thermal conductivity of 2.5W/m /°C as the average for igneous rocks and a Curie temperature of 580 °C (Stacey, 1977; Trifonova *et al*., 2009) are used as standard.

CHAPTER FOUR

4.0 RESULTS AND DISCUSSION

4.1 Interpretation of aeromagnetic data

The main aim of using the magnetic data is to outline the geological structures which are usually channels or means through which hydrothermal fluids are deposited and are important element in mineral exploration (Amenyoh *et al*., 2009).

Linear features in the granitoid, metamorphosed belt and basin rocks are observed as high magnetic anomalies. The concentration of magnetic minerals or their excessive destruction by alteration especially along tectonic structures allows the detection of geological structures

(Plumlee *et al*., 1992).

4.1.1 Total magnetic intensity map (TMI)

The magnetic anomalies of the study area as shown in (Figure 4.1) ranges from -114.4 nT minimum to 165.4 nT maximum. This Variation in magnetic susceptibility consisting of both positive and negative anomalies depicts the complexity of the structural geology of the area.aq The TMI map shows a distribution of high and low magnetic closures across the study area which are characteristic indications of trends such as difference in lithology, difference in magnetic susceptibility, variation in depth and degree of strike. The TMI map commences a relatively medium susceptibility region that occupies the northern end of the map down to Latitude 8.15°; this is immediately followed by a low magnetic susceptibility region that extends down to latitude 8.00°. On this low susceptibility region are observed some cringing surface features that are high frequency shortwave length magnetic closures both of high and low magnetic values. At the midpoint of the map is situated an E-W trending high magnetic signatures where a maximum susceptibility of about 165.4 nT was observed. The magnetic high values are

recorded around Lokoja where the old basement are quit exposed due to erosion. Major part of the lower end of the study area is occupied by low to average susceptibility except for a spherical high susceptibility at the Eastern corner on Latitude 7.15° that cannot be overlooked.

4.1.2 TMI reduce to equator map (RTE)

The RTE map was computed from the TMI map and it helped in achieving the symmetry for anomaly that exhibit dipolar nature due to non-vertical inducing field. The method also places the anomalies from the residual field directly above the causative bodies. (Figure 4.2) shows both positive and negative anomalies coming from magnetic rocks within the study area. The sedimentary rocks at the lower region of Koton-Karfe and Idah shows low susceptibility due to overlay of sedimentation. The basement rocks at the middle portion of study area depicts appreciably high susceptibility which is as a result of activities of intrusive bodies such as undifferentiated granite, Migmatite, Porhyritic granite and banded Gneiss.

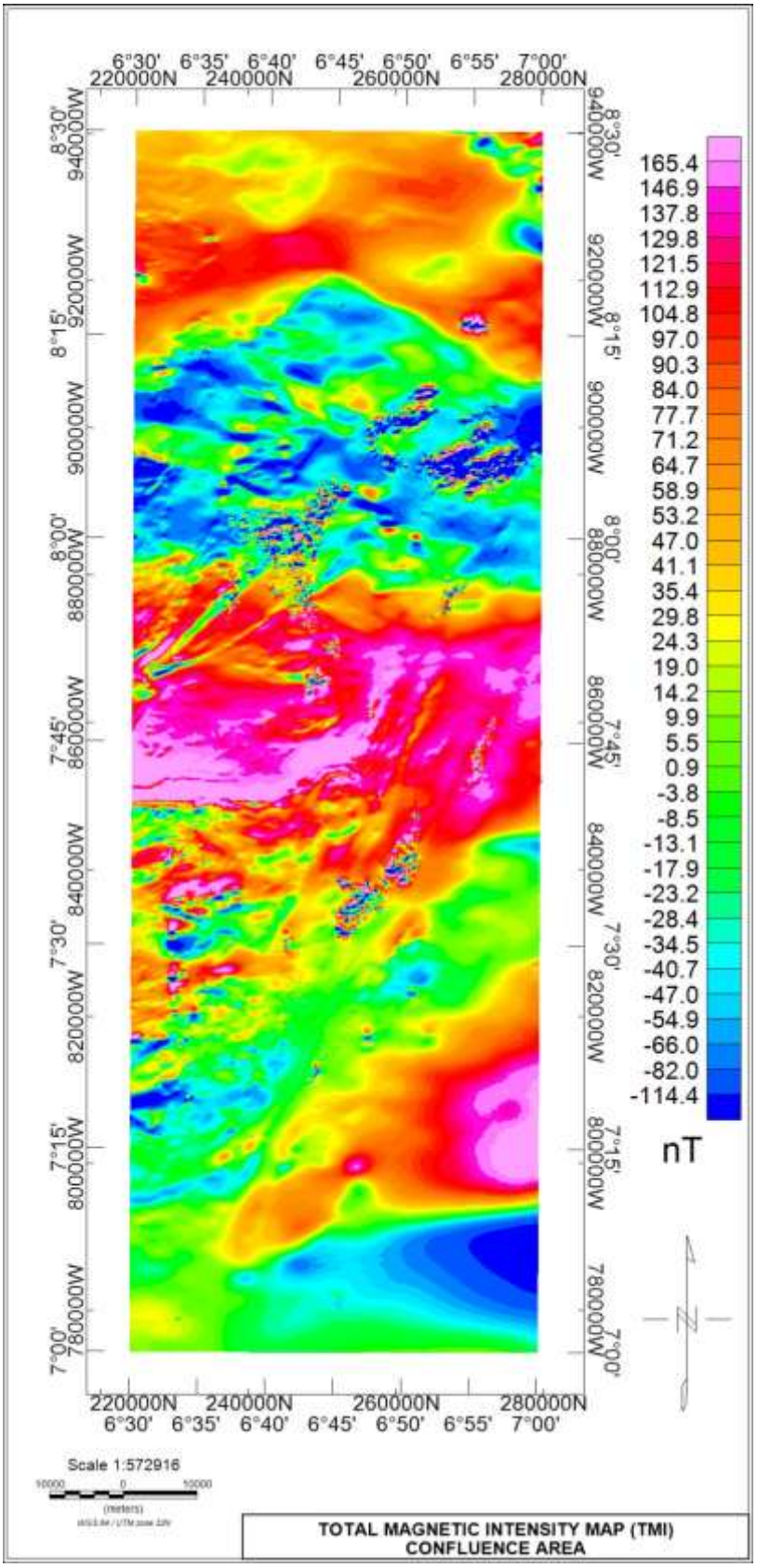

Figure 4.1: Total magnetic intensity map (TMI**)**

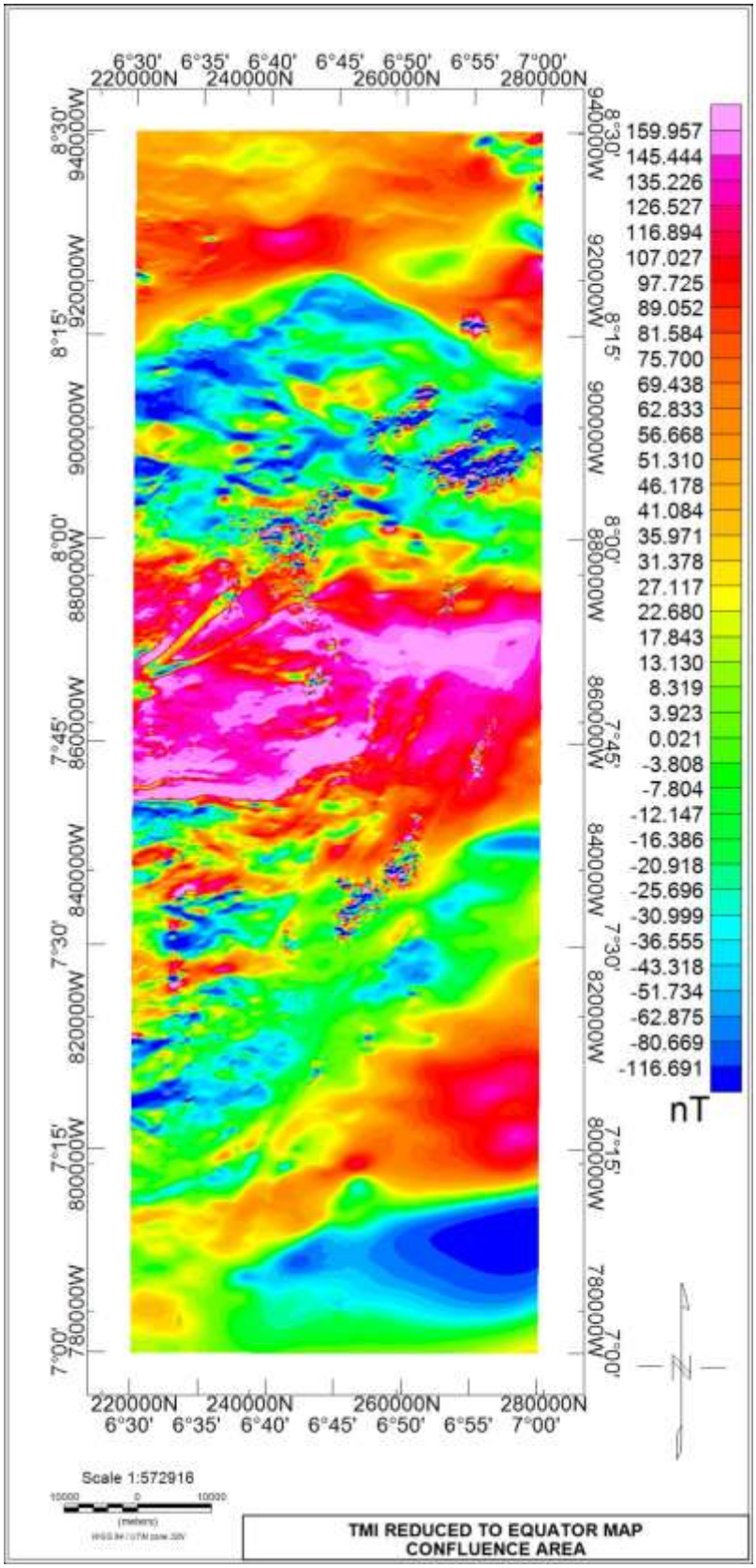

Figure 4.2: Reduced to equator map (RTE)

4.1.3 Horizontal derivatives (DX, DY, DZ)

The horizontal derivatives maps DX (Figure 4.3a), DY (Figure 4.3b) and DZ (Figure 4.3c) shows a clear demarcation between the region of basement and sedimentary rocks base on degree of distortion to magnetic signatures. The NW and SW portion of the area is covered by highly distorted short wavelength magnetic anomalous signatures that are the characteristic of outcrop and shallow intrusive magnetic bodies, while the remaining part of the study area (NE and SE) is characterized by medium to long wavelength magnetic signatures that are attributes of deep sited magnetic rocks in areas of medium to thick sedimentations.

The horizontal derivative (DX) shows magnetic signatures lying in Y directional axis while DY derivative shows magnetic signatures in X directional axis. DZ derivative portrays the both directions.

4.1.4 Analytical signal

The 3D Analytical Signal map (Figure 4.4) was generated from three orthogonal derivatives of the TMI (DX, DY and DZ). It is a data enhancement feature that is independent of the magnetisation field of the source rocks but rather dependent on the magnetisation amplitude of the causative bodies and hence its relevance in placing the magnetic anomalies over their causative bodies. Liu and Mickey (1998) indicated that high analytical signal amplitudes are recorded around areas of large mineral deposit.

The Analytical analysis showed high amplitude of susceptibilities across the field, though majorly within the basement regions but some isolated structures were discovered to be located within the sediments such as that between Latitude 8°00’ and 8°15’ above and within Koton-karfe. Idah is on low amplitude while the granite below Lokoja depicts high

amplitudes. High amplitude of susceptibilities ranges from 0.175 to 0.475 cycles (displayed in pink and red), while Medium and low amplitudes ranges from 0.003 to 0.160 cycles (displayed in yellow and green colours respectively).

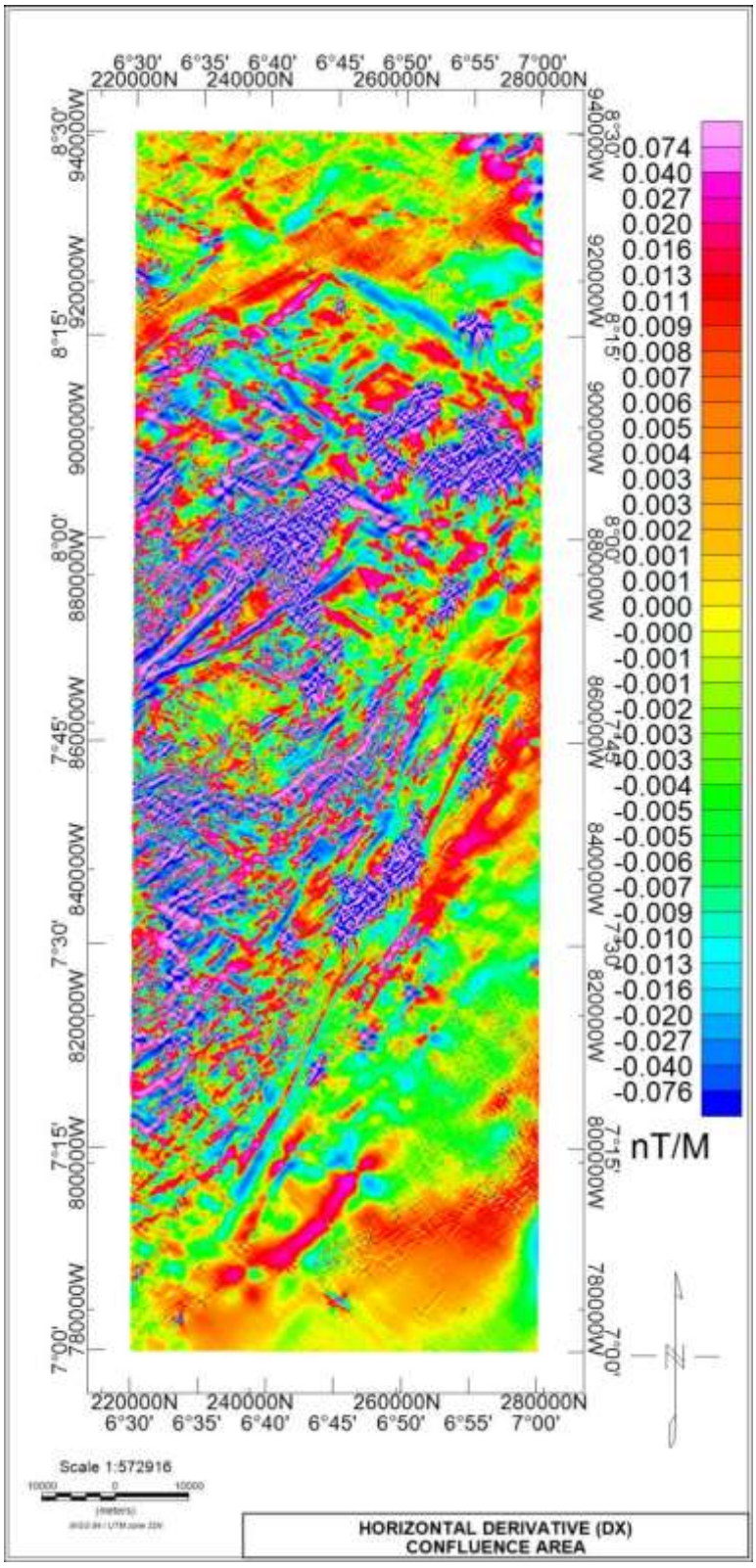

Figure 4.3a Horizontal derivative DX

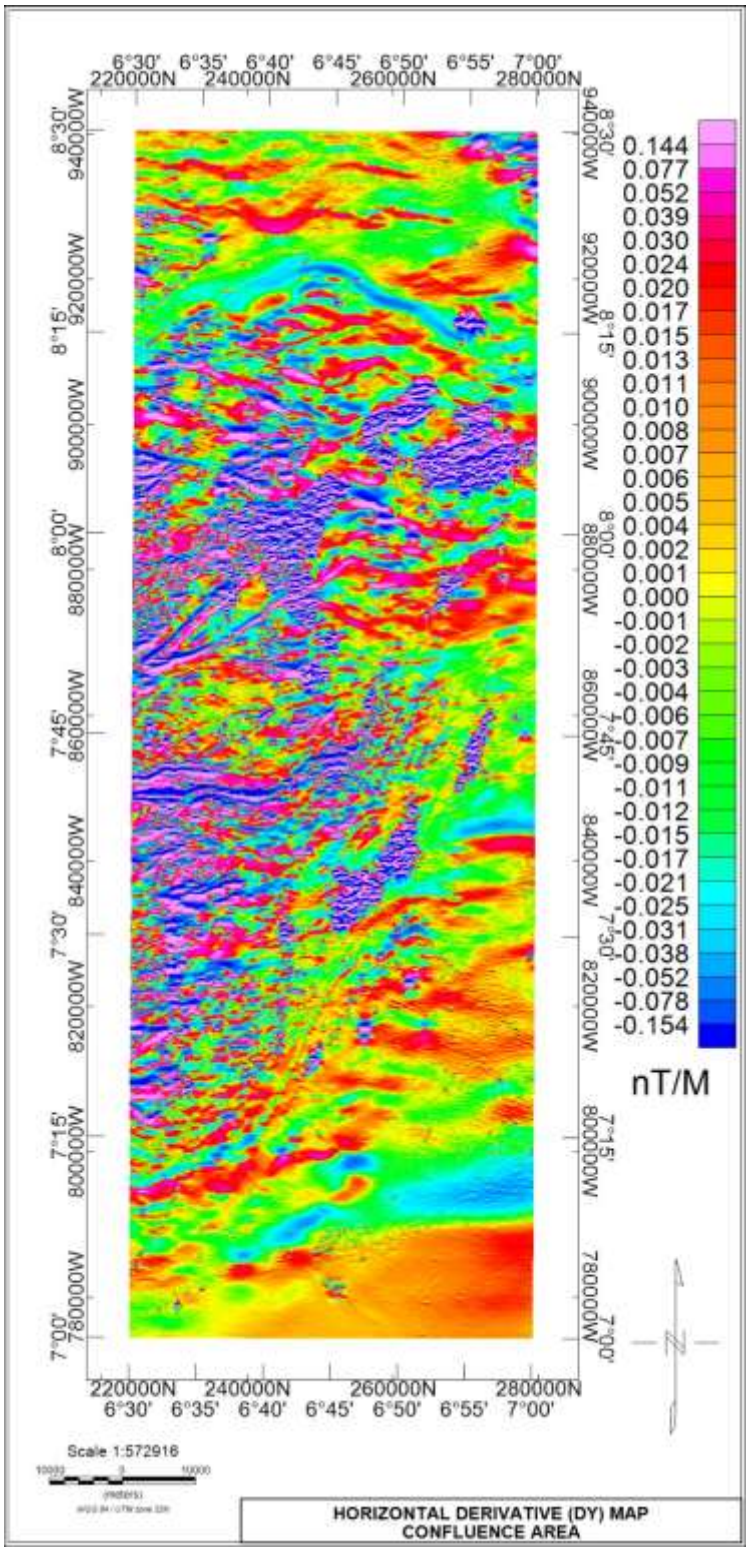

Figure 4.3b Horizontal derivative DY

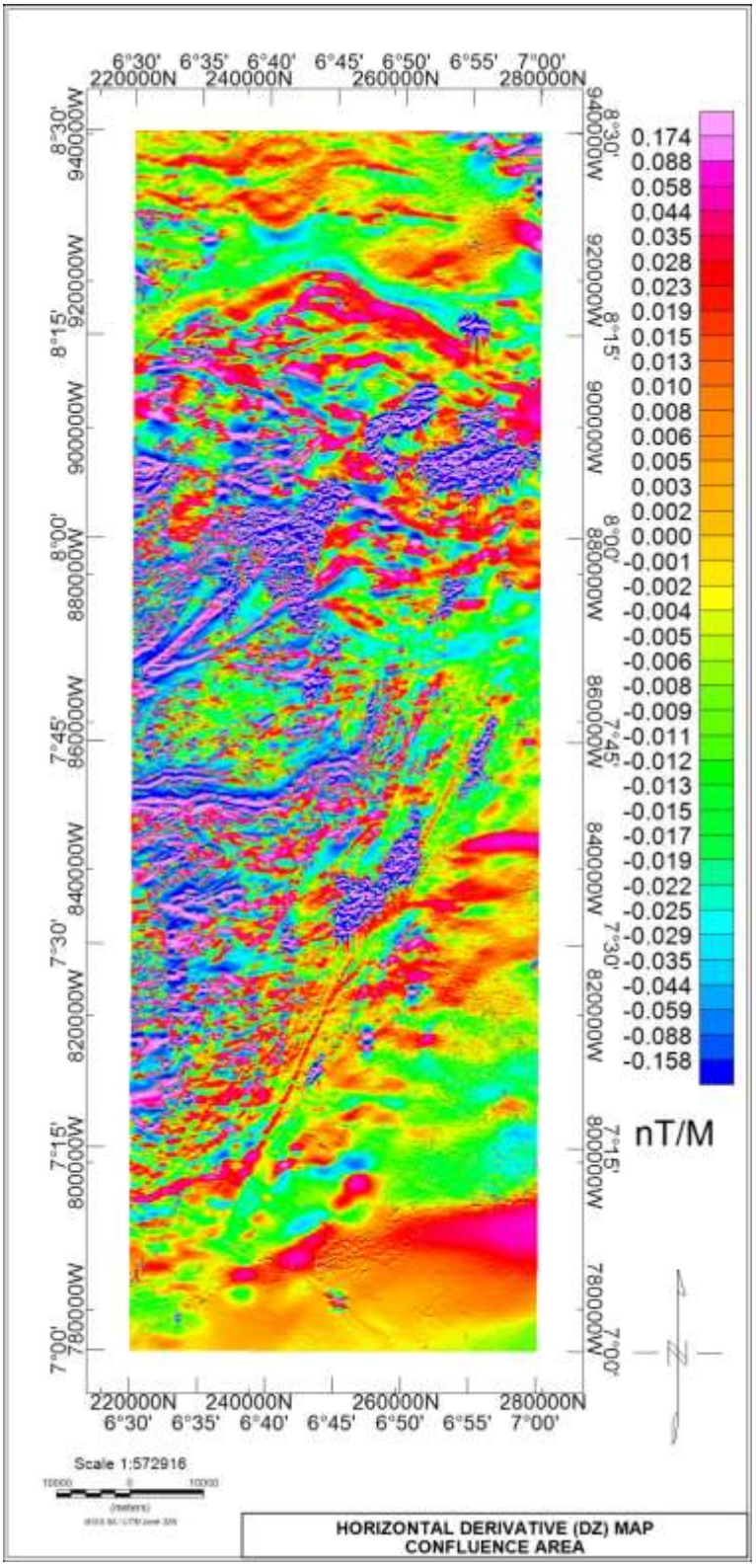

Figure 4.3c Horizontal derivative DZ

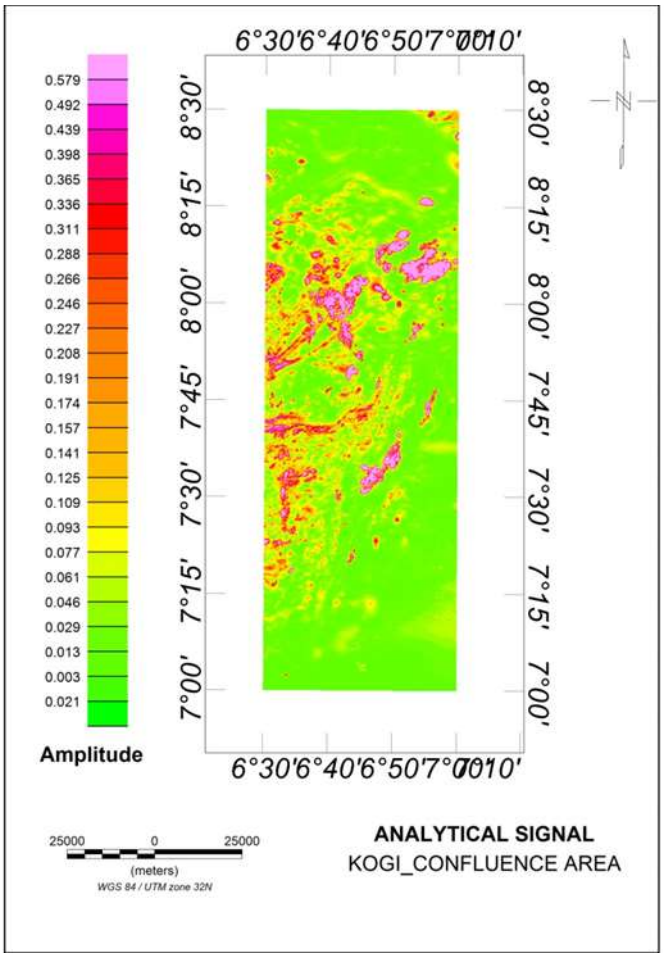

Figure 4.4 Analytical signal map

4.1.5 First vertical derivative (1VD)

The first vertical derivative map (Figure 4.5a) displays magnetic structures that can be related to the geology of the area. The contact between the sedimentary formation of Nupe Basin and South-Western Basement complex is defined by set of folds around Latitude 8.15° cutting across the entire study area horizontally. Below this are sets of cringing surface features B1 and B2 observed on the Total Magnetic Intensity (TMI) map just above Koton-karfe appearing as a mixture of both high and low susceptibilities, an intrusion of oolitic iron ore within the sedimentary formation. A similar surface feature B3 is captured at Adana (lower end of Lokoja) area overlaid by undifferentiated schist.

Between Latitude 7.45° to 8.00° are sets of linear structures (F2 and F3) trending in the NE-SW direction. These sets of structures extend down to Koton-karfe area from Tajimi, Emu and Agbaja in the SW region of study area. The structures (lineaments) also define contacts between the Migmatite, the Porhyritic granite and the Banded Gneiss. A set of E-W trending linear structures F4 and F5 both of high and low susceptibility are situated on Latitude 7.40° at the Western part of the study area. These structures are located within the Migmatite and extending into the undifferentiated granite and into the Schist belt across the river Niger around Kuroko, Koji and Chita. The major (in length) lineament F6 in the study area is a diagonally NE-SW trending fault line taking off from the Limestone at Iyanipodi through shale at Adam and Egomicha into the undifferentiated Schist at Opada, Agbajo and Olowo.

Figure 4.5b is the greyscale of the first vertical derivative, the structural view of the grey scale though having a resemblance of physical structures, is only a representation of magnetic signatures and not actual shape or appearance of rocks. Both the coloured and grey 1VD maps are similarly enhanced to make clearer geological structures which are not very obvious on the TMI map.

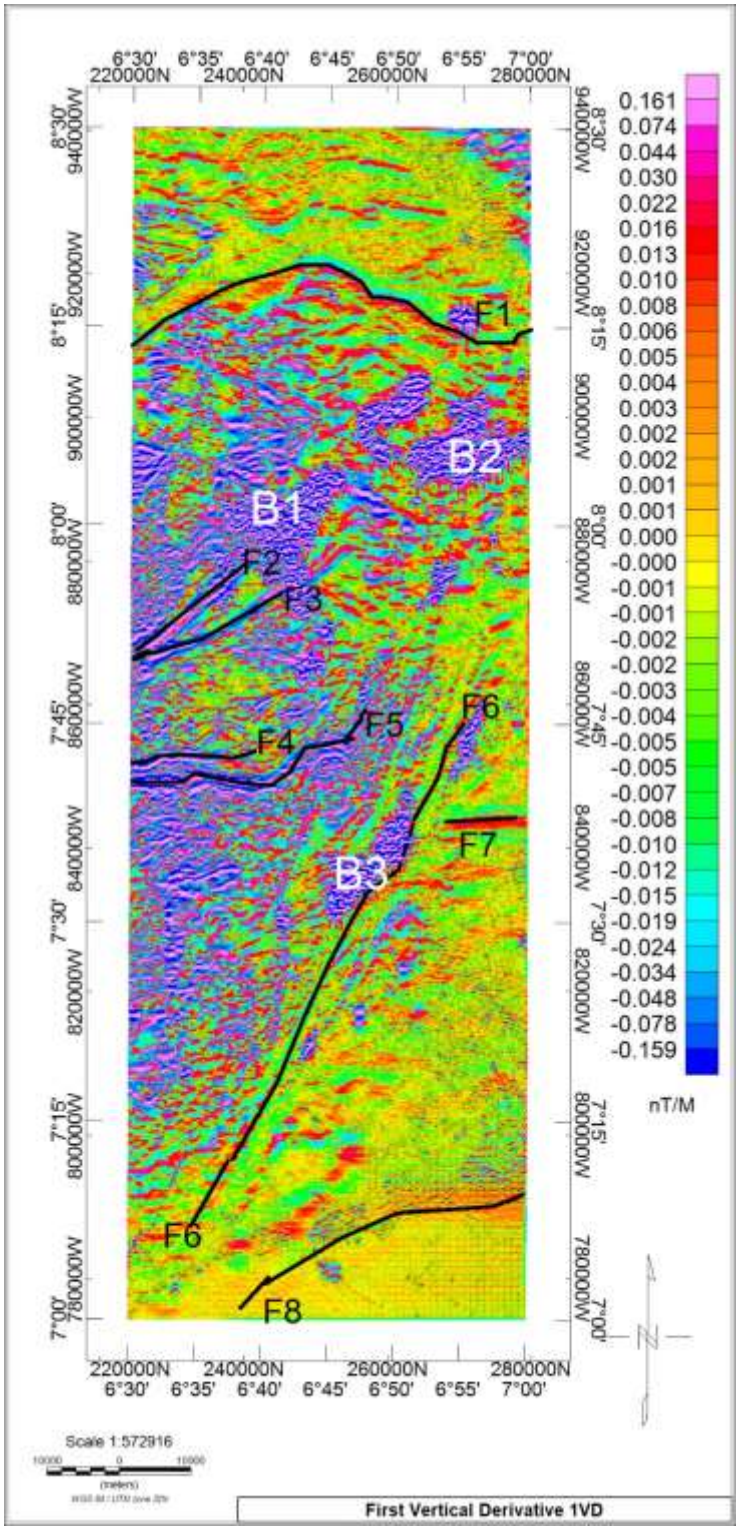

Figure 4.5a: First vertical derivative map (1VD)

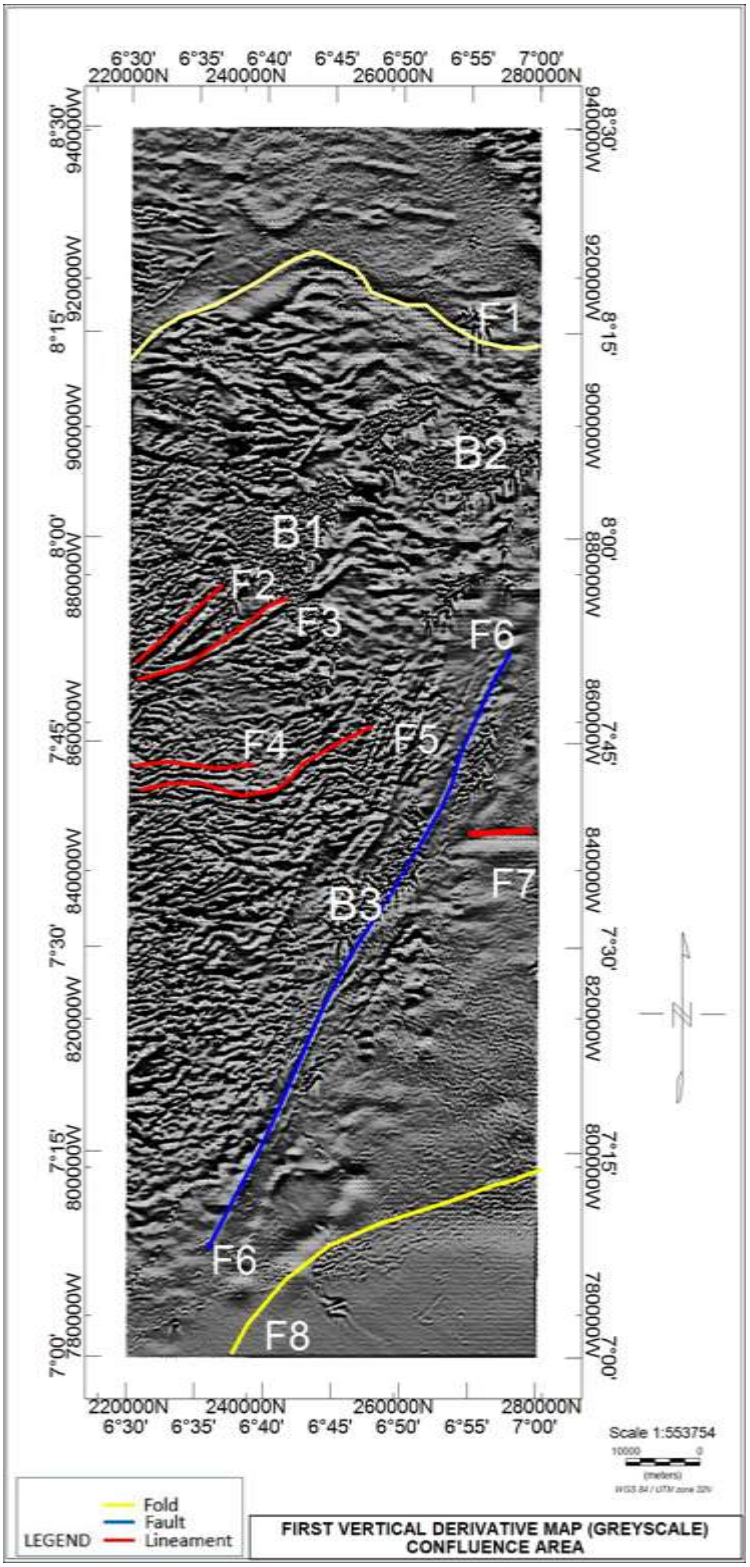

Figure 4.5b: First vertical derivative grey scale map

4.1.6 Centre for exploration targeting (CET)

An automatic algorithm that detect, attenuate, vectorise and lineate structural features within a spatially ordered set of gridded data is assembled into a module called CET. Results from this module is mapped in (Figure 4.6). Structures delineated and mapped are massive which is a reflection of the complex geology and degree of deformation that has occurred in these regions (NW and SW). Major lineament mapped coincide with regions where amplitude response from analytical signal are relatively high among which are the E-W trending lineaments within the migmatite down into the undifferented granite at a point where river Benue joins the river Niger; also a set of NW-NE trending linear structures is located within the contact between the Migmatite, the Banded gneiss and the Porphyritic granite which are clearly mineralised zones. The Northern end of the study area from Abaji down to Konton-karfe which is delineated sedimentary formation consisting of shale, limestone and sandstone as indicated by the geology map is also not entirely devoid of minor structures. Principally around Koton-karfe are bands of short wavelength closures with high magnetic susceptibility that appear like cringing surface structures but have been covered by sedimentation. This is understandable as the region is an area of depression created by the major fault line that define the course of river Niger (Adetona and Abu, 2013). Though the lineaments from CET correlates with those delineated in 1VD but it's detail in analysis.

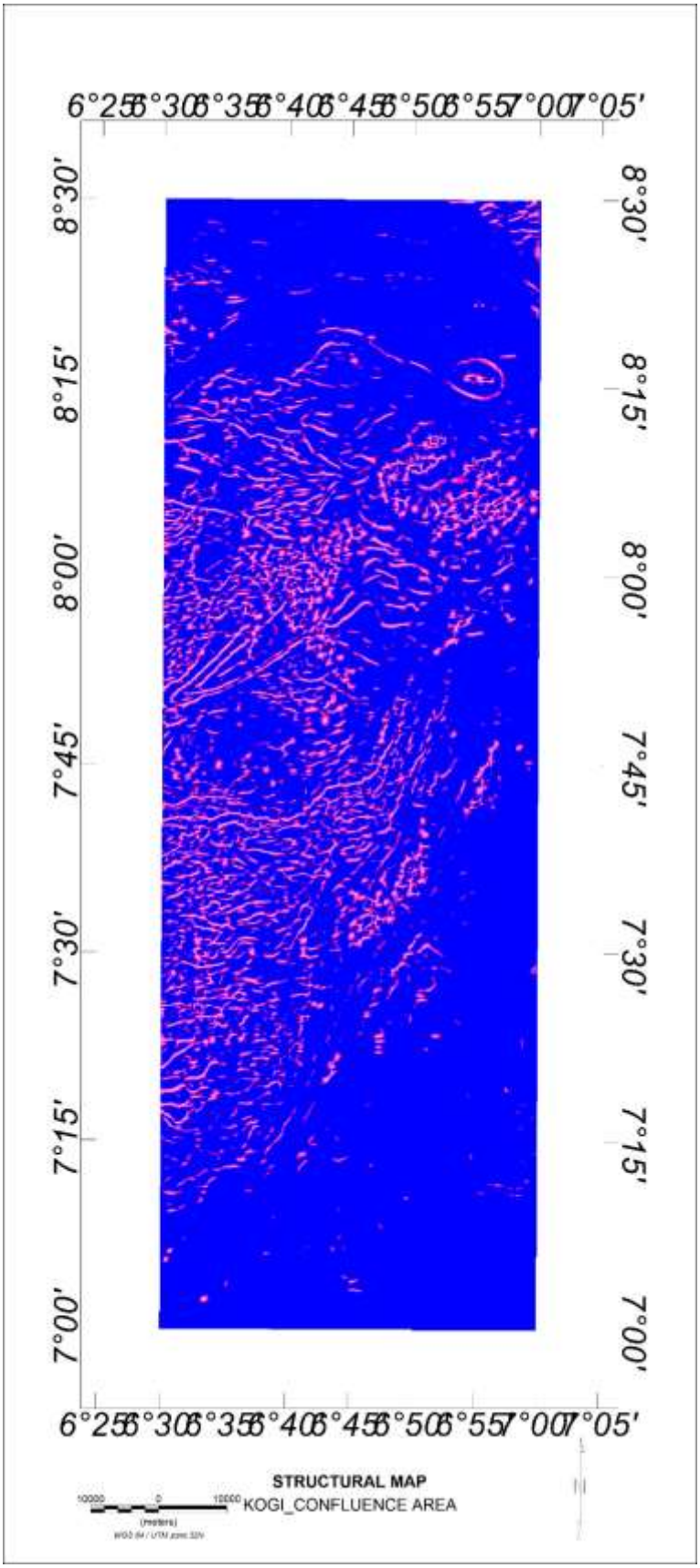

Figure 4.6: Centre for exploration targeting (CET) structural map

4.1.7 Euler deconvolution

The Euler depth map (Figure 4.7) establishes the general distribution of depth to magnetic sources in the study area. The mapped area is lithologically separated into two major components of Nigeria geology and is occupied by the south western basement from the NW down to the SW, part of the Northern and Southern region is encroached by the Nupe and Anambra basin respectively. The two basin geologies are covered by thick sediments hence the greatest depth to sources is observed in these sedimentary regions. Moderate to shallow depth to magnetic sources was observed around the basement regions as most of the basement rocks are situated as outcrops or at shallow depth below the surface. A moderate to high depth range of 670 to 1252 Metres was observed from middle portion to lower end of Koton-karfe, this range agrees with that obtained by (Olaseinde *et al.*, 2012). The thick depth to basement is associated with several outcrops of the sandstones sections along the Lokoja - Abaji Road preserved by a hard indurate top layer of laterite (Akanmu, 1998).

The magnetic sources response in the sedimentary South to South-Eastern region are sparsely packed due to little or no magnetisation associated rocks in the sedimentary regions dominated by shale and mudstone, a similar situation is also observed in part of the Northern region encroached by Nupe basin and occupied mainly by feldspathic sandstone and siltstone.

The NW and SW parts of the study area have closely packed mixture of shallow to moderate depth range response of magnetic sources as a result of basement rocks that are magnetically susceptible. The structures B1, B2 and B3 delineated on the 1VD which also appeared prominently on Analytical Signal maps are associated with depth range of

approximately 1252 Metres and above which also represent the greatest structural depth of the study area.

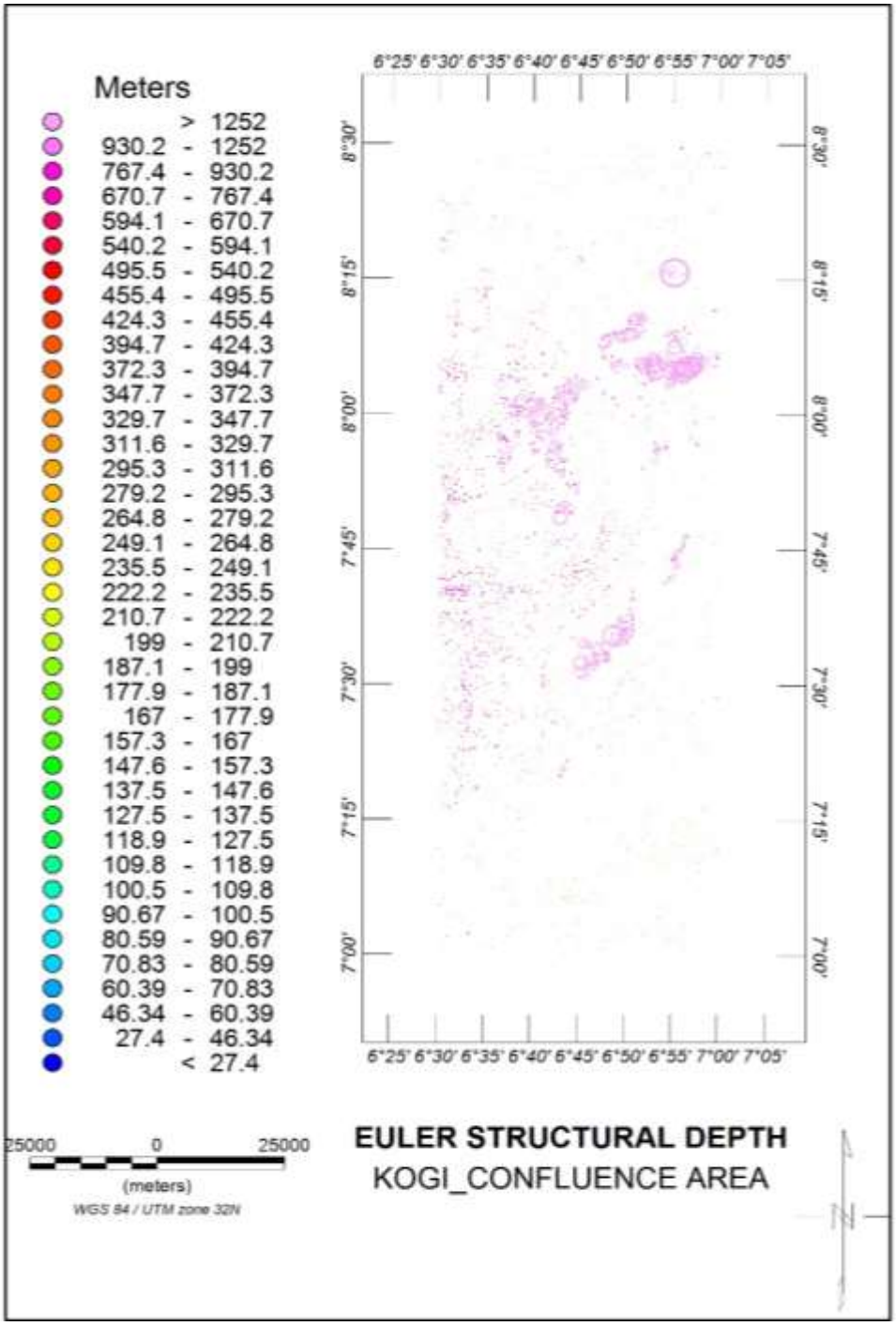

Figure 4.7: Euler structural depth map

4.2 Radiometric data interpretation

Gamma-ray spectrometry can be effective in geological mapping and targeting mineralization. The results depend on several factors, including whether:

i. There are measurable differences in the radioactive element distributions that can be related to differences in host rock lithologies,
ii. The potassium content of the rock has been modified by alteration processes, and
iii. Mineralization and alteration have affected surface rocks.

Mobilization of individual radioelements in response to specific geochemical conditions makes radioelement ratios sensitive in locating areas of mineralization (Thomas *et al.*, 2000). Images generated from the radiometric data set was analysed and interpreted to proffer geological meanings. High radiometric element patterns and irregular magnetic signature zones are interpreted to have resulted from possible mineral deposits or rock alterations (Gunn *et al.*, 1997).

4.2.1 Potassium (K), Thorium (Th), and Uranium (U) Channels

The three radioactive elements concentration channels clearly distinguish the lithological formations of the study area. While potassium highs were recorded at regions of basement felsic rocks in the western part of the study area, Thorium and Uranium had their highs at the regions dominated by sediments characterised by sandstones, clay, shale, limestone and mudstone.

The potassium map of study area (Figure4.8a) indicates the levels of potassium concentration and distribution across the area. Potassium radiation fundamentally emanates from potash feldspars which are mainly common in felsic igneous rocks such

as granite. (Gunn *et al.,* 1997). Both high and low concentration of potassium in percentage is visible across the study area displayed in colours. Peak values are shown in pink and red while low values are show in green and blue colours. High to relatively high concentration of potassium is dominant in the North-west down to South-western part of the study area. These regions falls into the Western Nigeria basement geology characterised by Migmatite, Banded-gneiss and Porphyritic granite. The NE and SE records significantly low concentration and is in the sedimentary part of the region encroached by Nupe and Anambra basins respectively. Thorium (Figure 4.8b) and Uranium (Figure 4.8c) have their high values in the NE region of study area. Also worthy to note is a low for K and high concentration for Th and U observed at the western edge Latitude 7.45°.

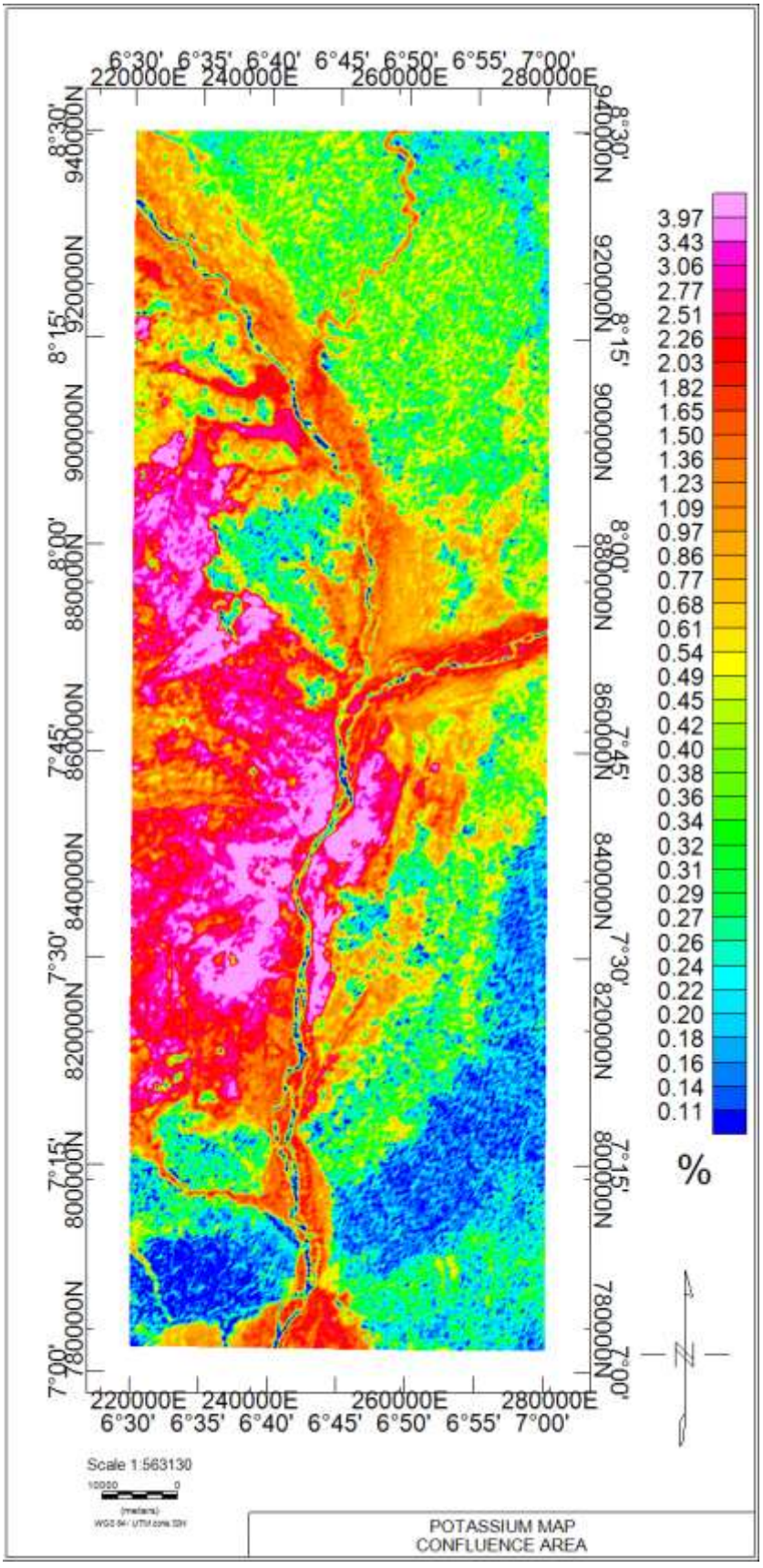

Figure 4.8a: Potassium concentration map

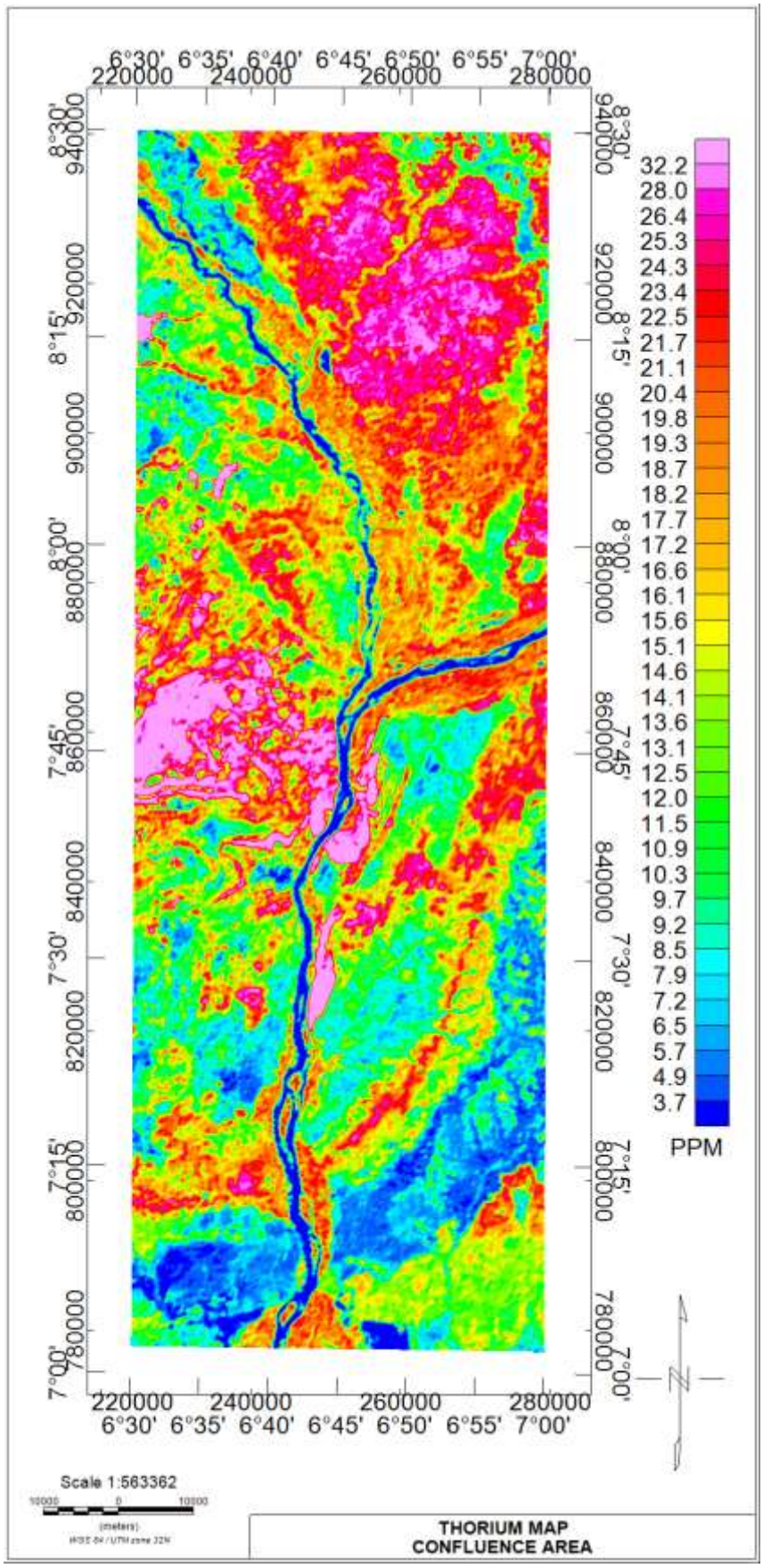
6°30' 6°35' 6°40' 6°45' 6°50' 6°55' 7°00'
220000 240000 260000 280000
8°30' 940000
8°15' 920000
8°00' 900000
7°45' 880000
7°30' 860000
7°15' 840000
7°00' 820000
780000
32.2
28.0
26.4
25.3
24.3
23.4
22.5
21.7
21.1
20.4
19.8
19.3
18.7
18.2
17.7
17.2
16.6
16.1
15.6
15.1
14.6
14.1
13.6
13.1
12.5
12.0
11.5
10.9
10.3
9.7
9.2
8.5
7.9
7.2
6.5
5.7
4.9
3.7
PPM
Scale 1:563362
(meters)
THORIUM MAP
CONFLUENCE AREA

Figure 4.8b: Thorium concentration map

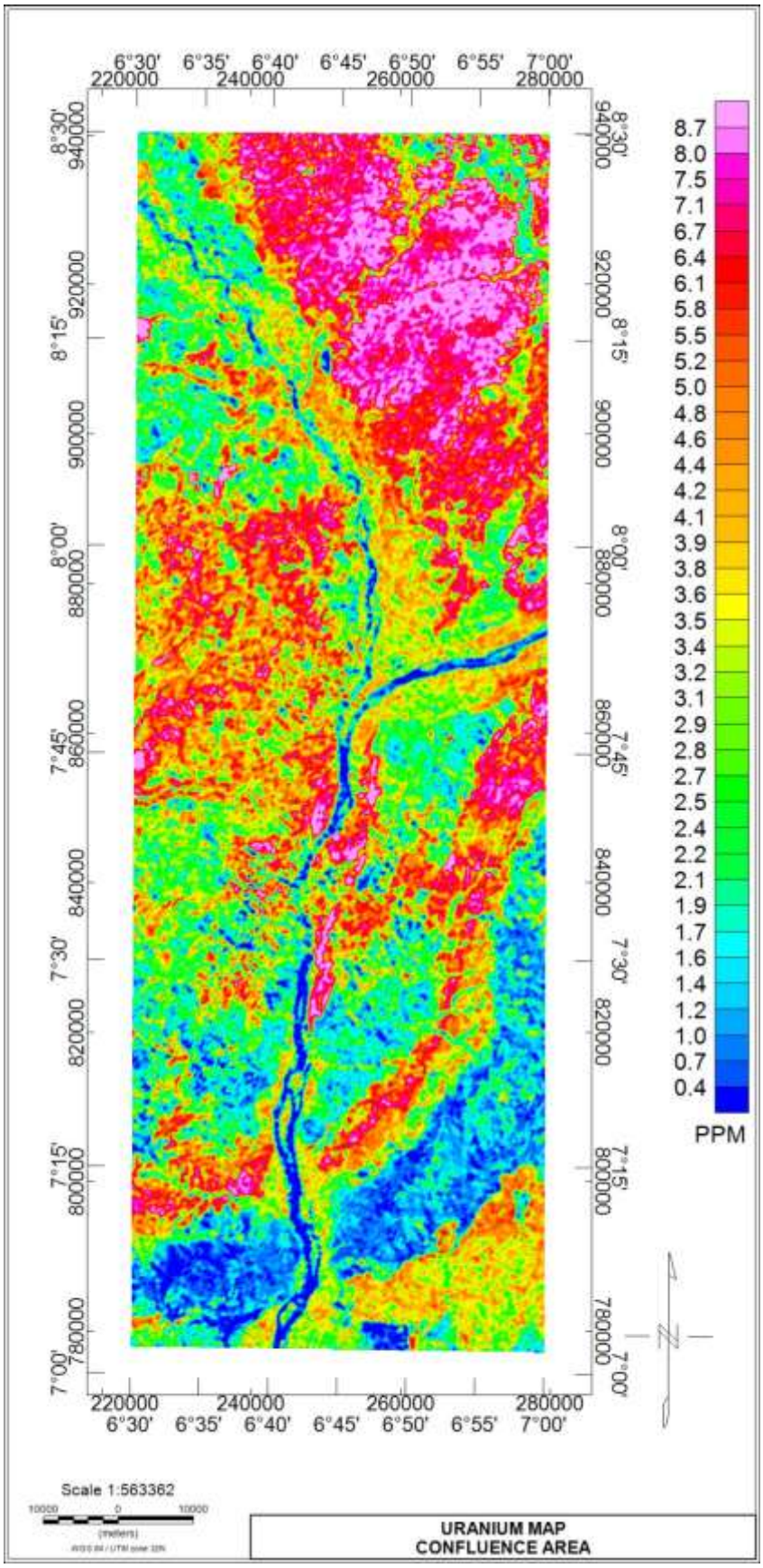

Figure 4.8c: Uranium concentration map

4.2.2 Ratio maps of K/Th, K/U, Th/K, Th/U and U/K

The ratio maps were useful in understanding the degree to which the source rocks were weathered or leached since K responses is associated with easily weathered minerals while Th and U are related with clay, oxides and accessory minerals (Wilford *et al*, 1997)

Radiometric signatures from radioelement ratios are essential for detecting the enrichment or depletion of particular radioelement over the other. Mappings from radioelement ratios can proffer clear indications of hydrothermal alterations in rocks as it is a process that leads to the deposition and enrichment of one element at the expense of the other. (Schwarzer and Adams, 1973). Due to the more mobile and soluble nature of K compared to Th, hydrothermal alteration processes usually leads to the enrichment and deposition of K-bearing minerals while Th is deficient from the components added to host rocks. Hoover *et al.* (1992) and Portnov (1987) gave the range of values for the K/Th ratio content of rocks that have not undergone alteration process to be between 0.17 %/ppm to 0.2 %/ppm. Anomalous values outside this range is attributed to K or Th specialised rocks (Portnov, 1987). The K/Th ratio map Fig (4.9a) shows clear indications of hydrothermally altered regions portrayed by values above stated threshold (0.2 %/ppm) shaded in pink colour. The regions around Latitude 8°00’ and 7°30’ within the NW and SW respectively were mapped on the K/Th ratio map with colour shades of pink to be the areas to have undergone K enrichment due to hydrothermal alteration. The hydrothermally affected western regions of study area are characterised by felsic mineralized rocks such as; Migmatite, banded gneiss and porphyritic granite. The zones of alteration also corresponds to the areas delineated to host major magnetic lineaments of mineral potential trending NE-NW and E-W direction of study area.

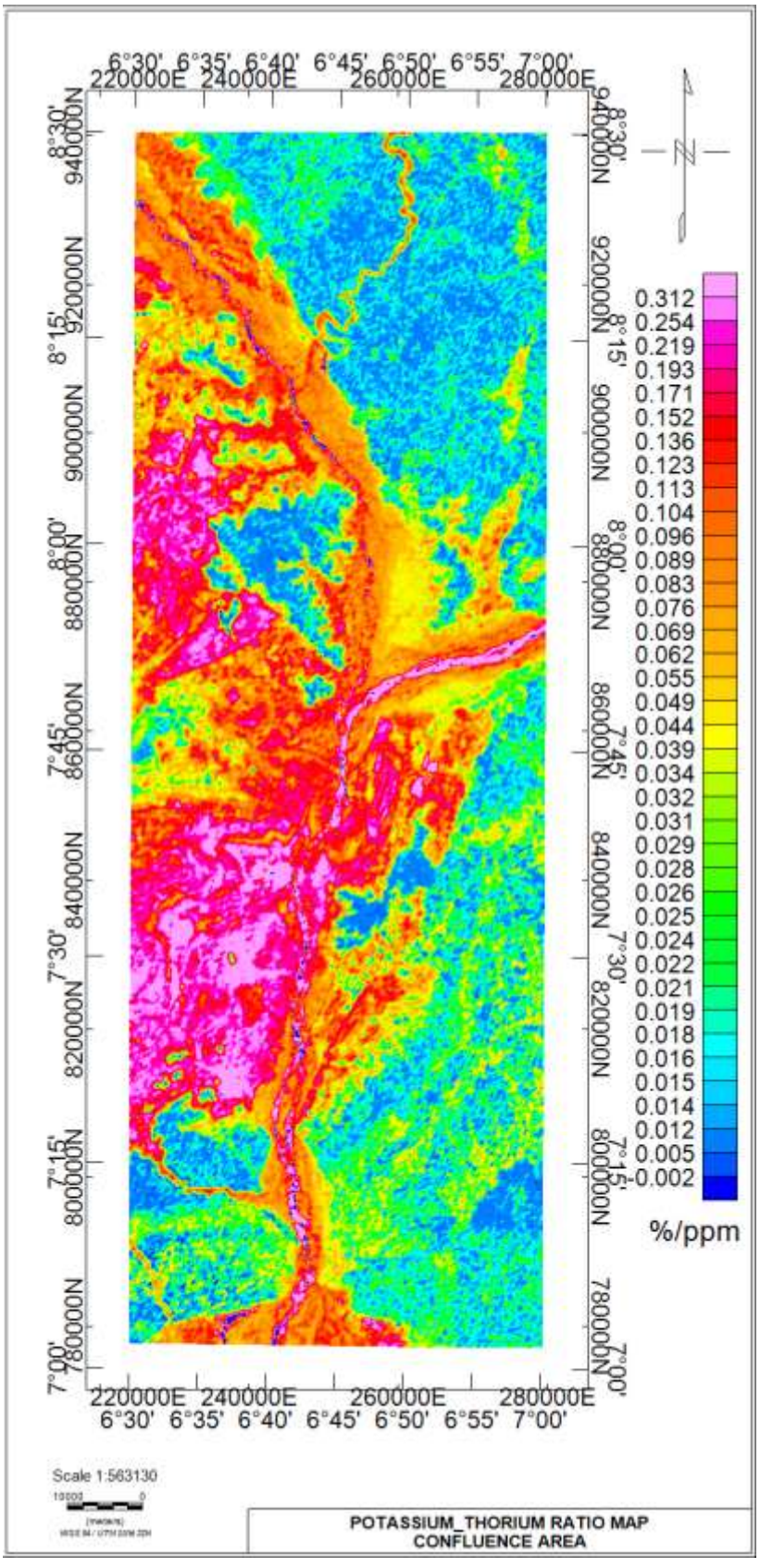
6°30' 6°35' 6°40' 6°45' 6°50' 6°55' 7°00'
220000E 240000E 260000E 280000E
8°30' 940000N
8°15' 920000N
8°00' 900000N
7°45' 880000N
7°30' 860000N
7°15' 840000N
7°00' 820000N
800000N
780000N
0.312
0.254
0.219
0.193
0.171
0.152
0.136
0.123
0.113
0.104
0.096
0.089
0.083
0.076
0.069
0.062
0.055
0.049
0.044
0.039
0.034
0.032
0.031
0.029
0.028
0.026
0.025
0.024
0.022
0.021
0.019
0.018
0.016
0.015
0.014
0.012
0.005
-0.002
%/ppm
Scale 1:563130
POTASSIUM_THORIUM RATIO MAP
CONFLUENCE AREA

Figure 4.9a: Potassium and thorium ratio map

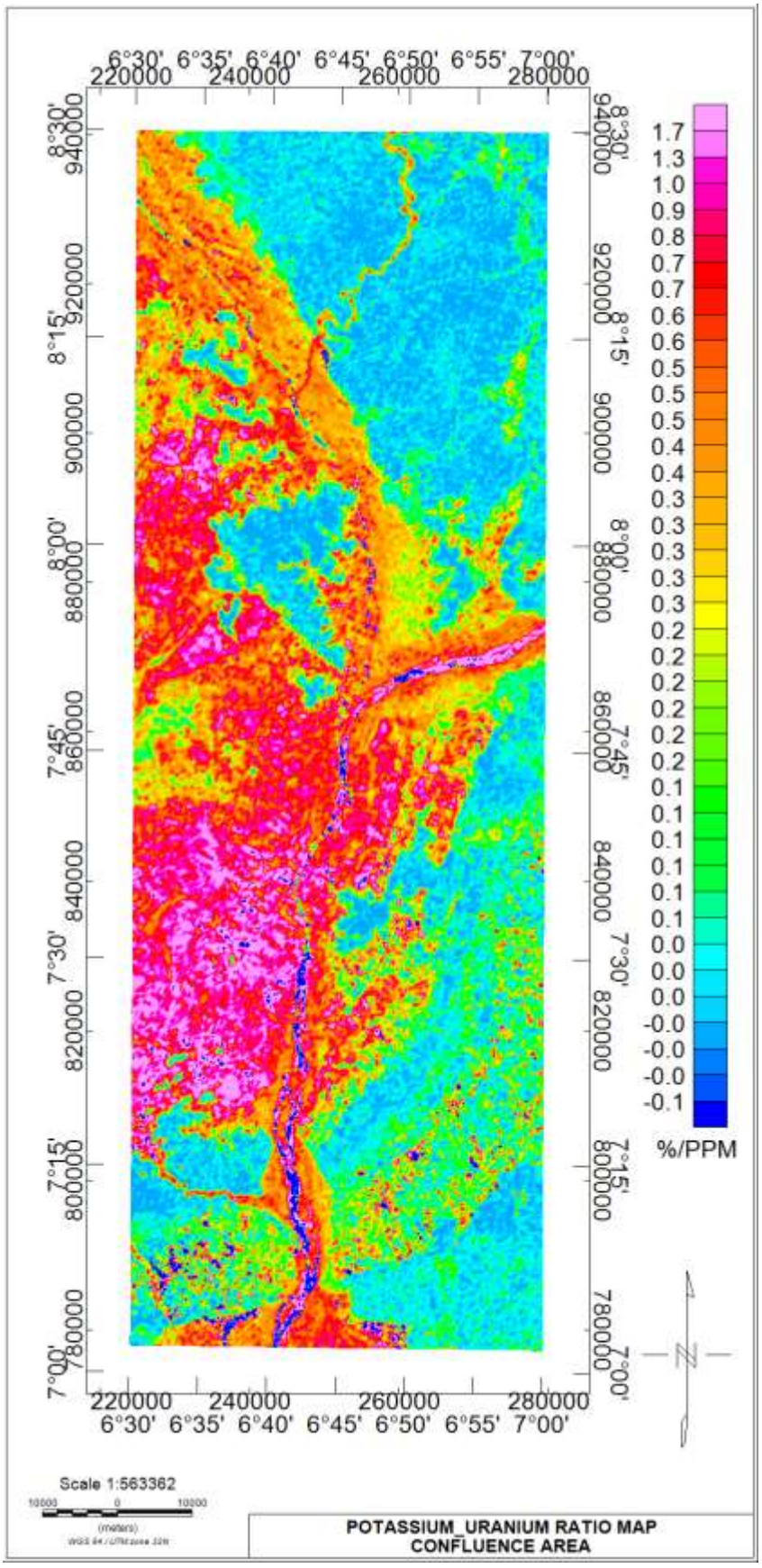

Figure 4.9b: Potassium and uranium ratio map

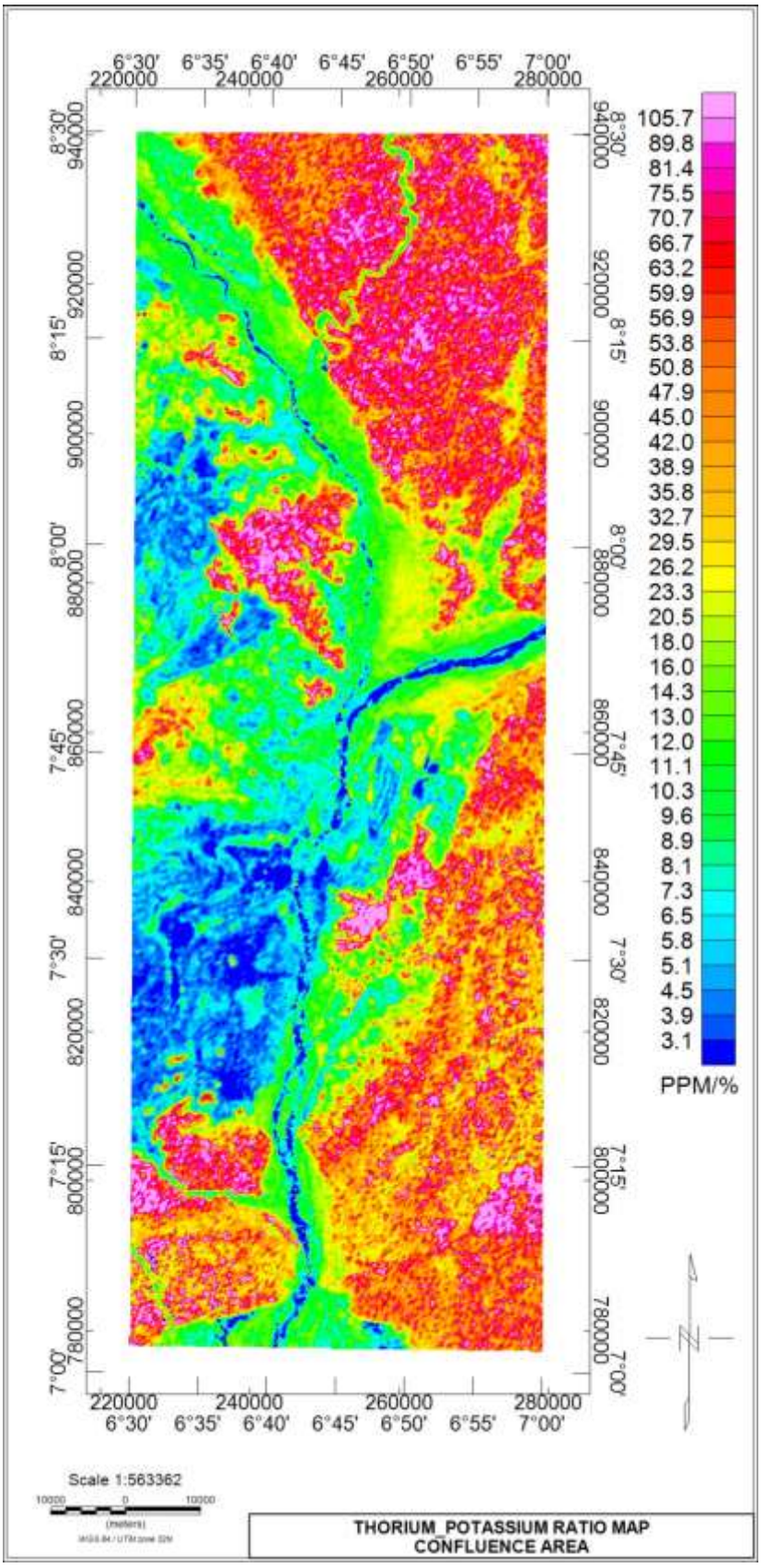

Figure 4.9c: Thorium and potassium ratio map

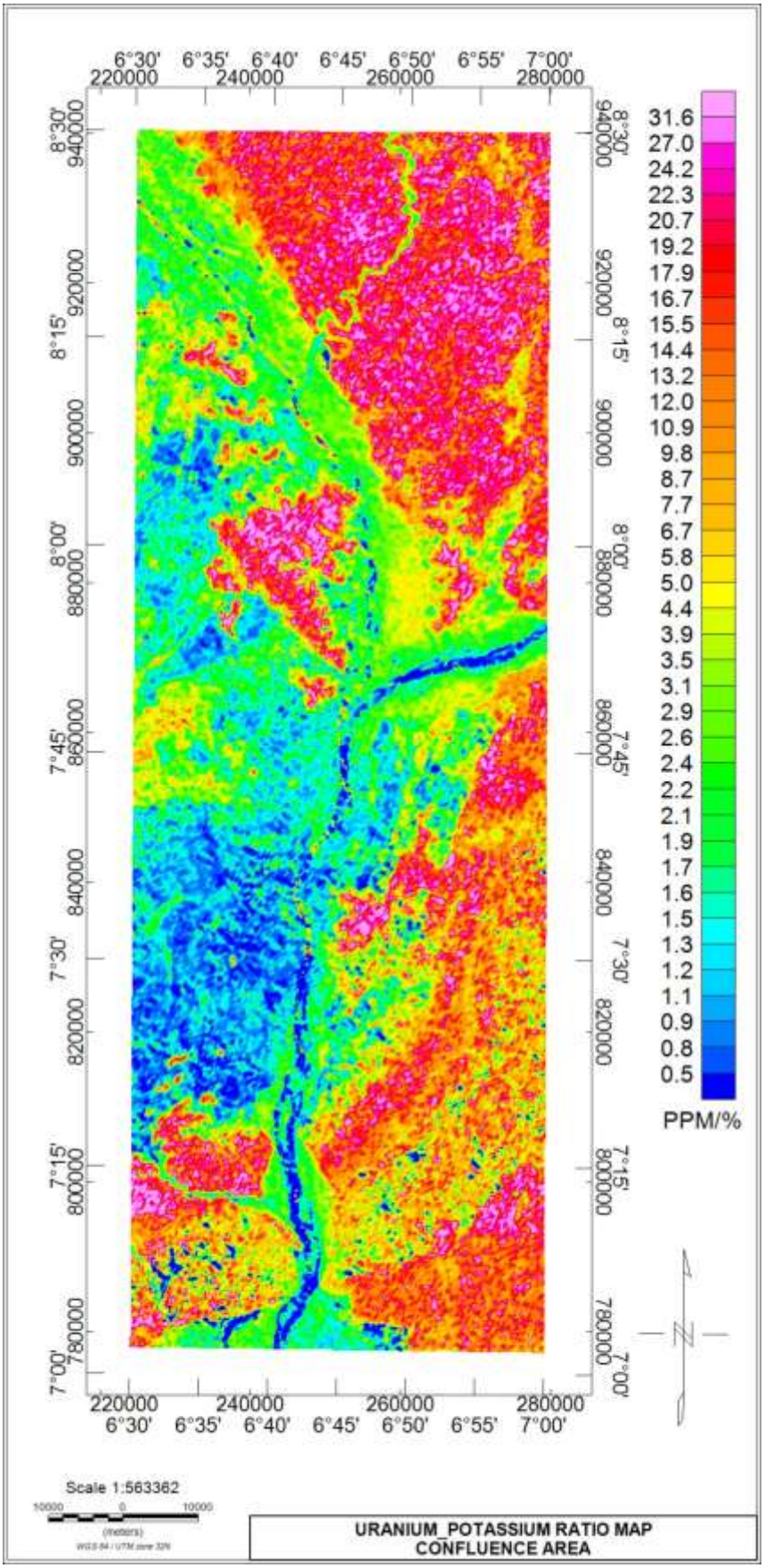
6°30' 6°35' 6°40' 6°45' 6°50' 6°55' 7°00'
220000 240000 260000 280000
8°30' 940000
8°15' 920000
8°00' 900000 880000
7°45' 860000
7°30' 840000 820000
7°15' 800000
7°00' 780000
31.6
27.0
24.2
22.3
20.7
19.2
17.9
16.7
15.5
14.4
13.2
12.0
10.9
9.8
8.7
7.7
6.7
5.8
5.0
4.4
3.9
3.5
3.1
2.9
2.6
2.4
2.2
2.1
1.9
1.7
1.6
1.5
1.3
1.2
1.1
0.9
0.8
0.5
PPM/%
Scale 1:563362
10000 0 10000
(meters)
URANIUM_POTASSIUM RATIO MAP
CONFLUENCE AREA

Figure 4.9d: Uranium and potassium ratio map

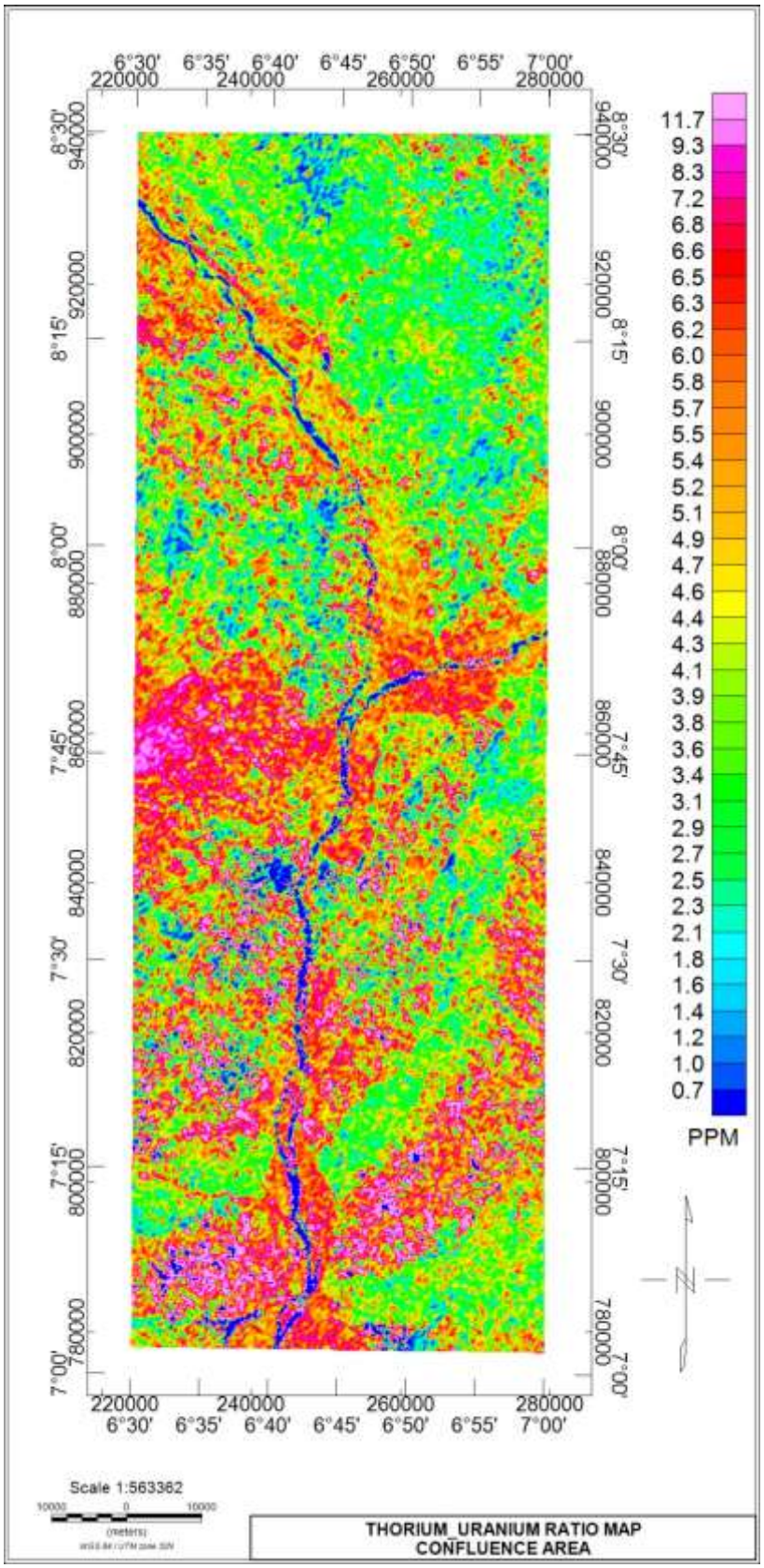

Figure 4.9e: Thorium and uranium ratio map

4.2.3 Ternary map

The Ternary image for the confluence area of Kogi state was computed using the RGB colour model and Histogram equalization colouring method. The image consists of colours produced from individual concentration of the gamma radiations corresponding to slight differences in the relative amounts of the components. Across the study area, regions with high concentration of the three radioactive elements (K, Th and U) are indicated as white while those in dark colours indicate low K, Th and U. Red is indicative of K dominance while Green and Blue colours indicates high Th and U respectively.

A clear blue colour dominating the North-Eastern corner of the study area is generally in the sedimentary region indicating high level of U and Th. This feature is associated with exposed iron stones gravel (Ramadas *et al.,* 2013)

Below the confluence of river Benue and Niger are regions of Brown to Dark Red colours, these are regions of granite and migmatite indicating high K and low concentration of Th and U. Observed on the western edge of study area at Latitude 7.45° is a bright green coloured feature which indicates relative high Th and U with low K, a feature that clearly indicates intrusion of granite into migmatite. The NW and SW regions coinciding with regions of migmatite and granitic rocks portrayed in dark red colouration are indicative of potassium feldspars presence (Ramadass *et al.*, 2013).

At latitude 8°00’ is an enclosed blue-green colour denoting and intrusion of feldspathic sand stones into the migmatite terrain, an area also observed as weathered basement on the TMI map showing mixture of high and low susceptibility.

Worthy to note on the ternary image are two giant strips of blue and dark colouration extending from the Eastern edge and curving in the south. The blue strip significantly indicates a contact between the encroaching Anambra basin in the South-East and the

basement geology in the Western part of study area. The blue strip is also associated with ironstone and sandstone as indicated on the geology map. The dark strip is a clear reflection of fluvial lithology in the sedimentary basin characterised by fika sandstone and clay as indicated by geology map. The dark strip also correlates to low concentration of the three radioelements which is attributed to varying geologic framework compositions, weathered materials or fluids formed as a result of intense metamorphism. (Ademila *et al.*, 2018). The river channel running from the North through to the South is depicted in dark colour reflecting low concentration of the three radiogenic elements. The low concentration along the water body is attributed to the fact that water bodies shield all radiations (Graham, 2013)

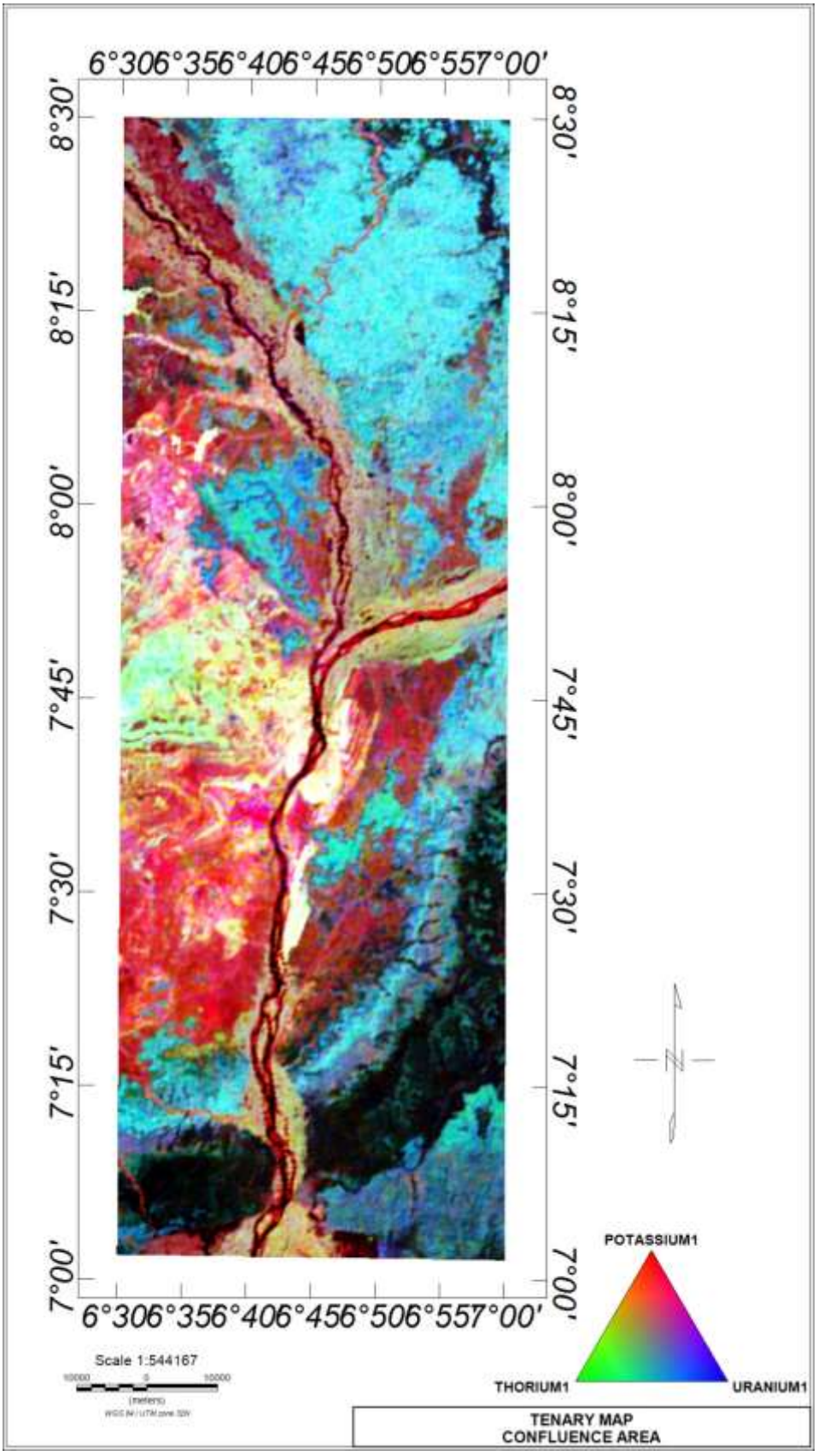

Figure 4.10: Ternary map

4.3 Spectral Depth Analysis

Spectral analysis was applied to the aeromagnetic data with the aim of determining the depth to basement as well as the basement morphology. The TMI was windowed into eight overlapping windows or sub-sheets. Each section of the windows was subjected to Fast Fourier Transform (FFT) and subsequently spectral depth analysis, a process which decomposes the anomalies into its energy and wave number components. A plot involving Energy versus wave number in cycle/km was made and a straight line of best fit was manually fit to the energy spectrum both in the higher and lower portion (Figure 4.11), this generated gradient G1 and G2 respectively which were further used to estimate the Heat flow, Geothermal gradient and Curie point depth of the study area seen in (Table 4.1).

The depth to magnetic sources at shallow depth (Z_T) occurred between 0.185 and 0.336 km while centroid depth varied from 4.46 to 12.09 km. (Table 4.1) A record of Curie depth (Z_B) across the study area varied from 8.69 to 23.98 km with and average value of 16.45 km. peak to medium CPD values were recorded at Idah (southern part) and koton-Karfe (norther part) respectively. Low CPD values of study area were recorded at the Lokoja (Middle region) area with the least value occurring at the western edge of Lokoja

Figure 4.11C shows distribution of geothermal gradient across the study area. The koton-Karfe area (Northern part) and Idah area (southern part) shows low values ranging from 24 to 34 °C/Km. The middle portion (Lokoja area) shows prevalence of high values with highest value occurring at the western edge of Lokoja area.

An anomalous Heat flow of range 100 to 166 mW/m2 was recorded across the middle portion of study area trending E-W of Lokoja region while values between 60 to 90 mW/m2 is shaded in green colour at the upper and lower regions of study area.

Table 4.1 Estimated values of the Curie point depth, geothermal gradient and heat flow

Sct	Lon (°E)	Lat (°N)	Grad (G)	Depth to Top Z_T (Km)	Grad (2)	Depth to Centriod Z_0(Km)	Curie Point Depth Z_B(Km)	Geothermal Gradient (°C/Km)	Heat Flow (mW/m^2)
1	6.625	8.125	135	0.25222788	3.17	10.74156588	21.23090388	27.31866732	68.29666829
2	6.875	8.125	117	0.18539147	2.33	9.309357097	18.43332272	31.4647559	78.66188976
3	6.625	7.375	102	0.336569064	4.23	8.115849777	15.89513049	36.48916254	91.22290634
4	6.875	7.375	107	0.303150859	3.81	8.513685551	16.72422024	34.68024169	86.70060422
5	6.75	8.125	99.9	0.229153405	2.88	7.948758752	15.6683641	37.01726589	92.54316474
6	6.75	7.375	152	0.20050923	2.52	12.09420751	23.98790579	24.178851	60.4471275
7	6.625	7.75	56.1	0.23154042	2.91	4.463717377	8.695894335	66.69814256	166.7453564
8	6.875	7.75	70.6	0.210057288	2.64	5.61744112	11.02482495	52.60854503	131.5213626

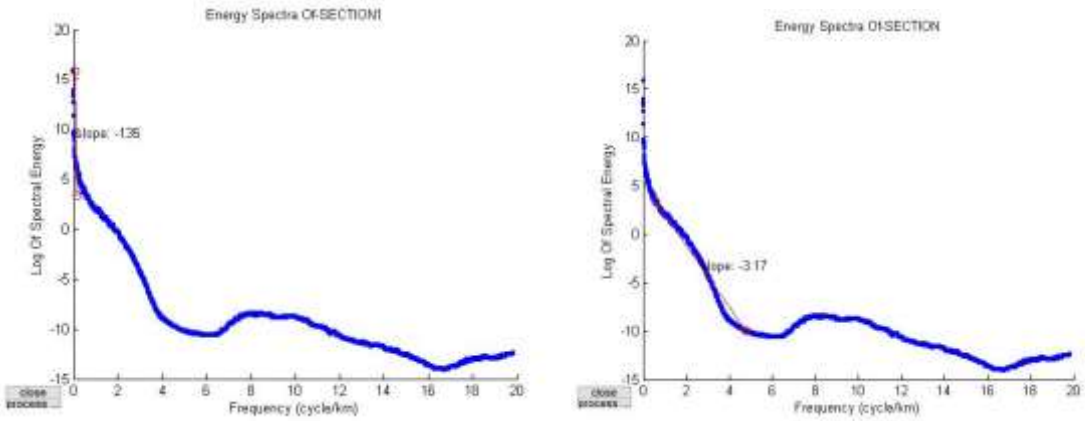

Figure 4.11: Graph of energy spectrum versus wave number for section one

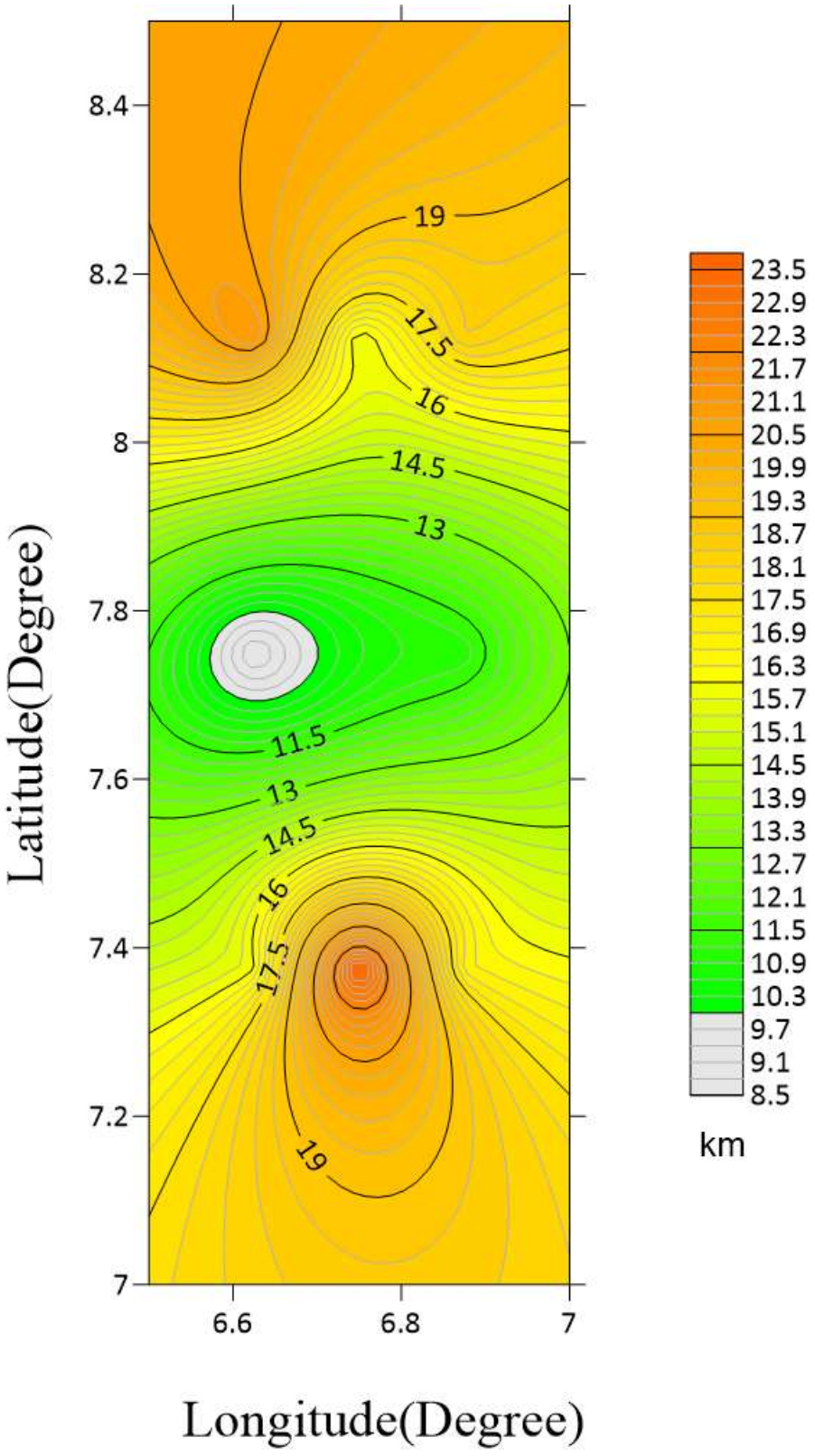

Figure 4.12a: Curie point depth contour map of study area

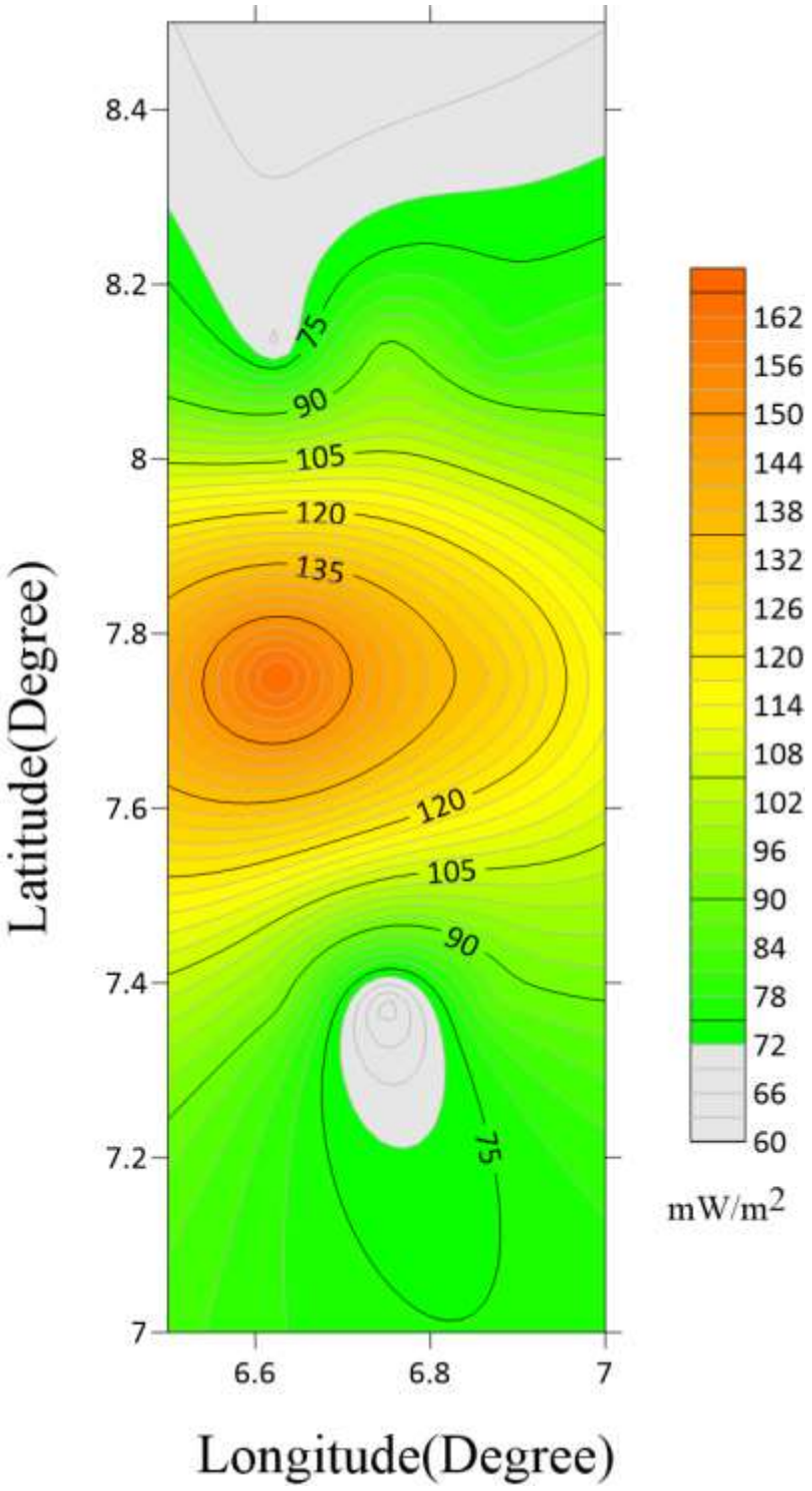

Figure 4.12b: Heat flow contour map of study area

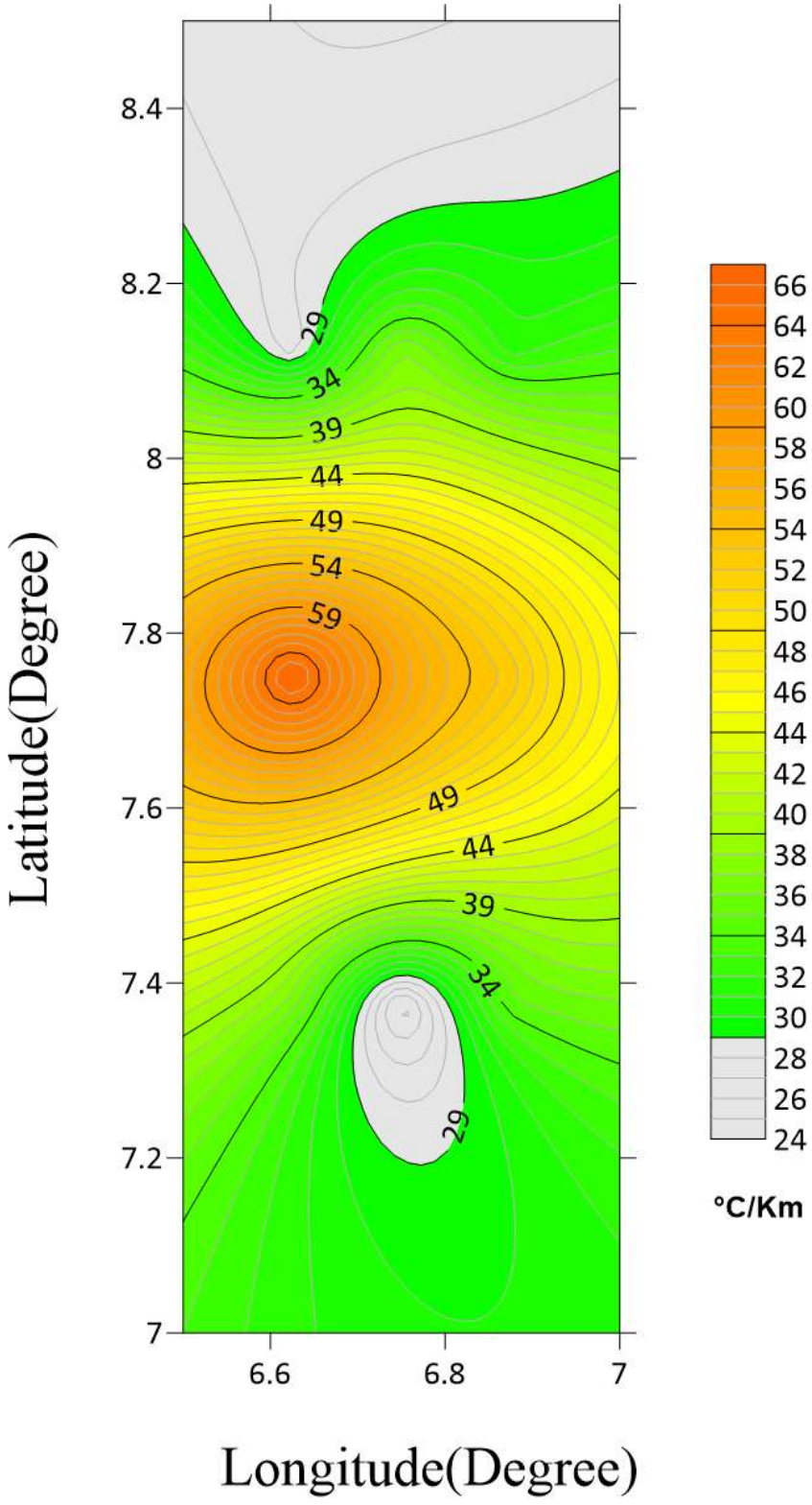

Figure 4.12c: Geothermal gradient contour map of study area

4.4 Discussions

The TMI showed regions of high and low magnetic susceptibility that relates to the geological setup of the study area.

The Horizontal derivatives revealed the boundaries of basement and sedimentary geologies that makes up the study area based on high and low distortion to magnetic signatures respectively. The basement and sedimentary geologies are associated with the Nigerian South western basement complex and the Nupe/Bida and Anambra sedimentary basins respectively. The basement geology was seen to be aligned in the western regions (NW and SW) while the sedimentary formations occurred majorly at the Northern region for Bida basin and southern region for Anambra basin.

The Analytical Signal showcased amplitude response that corresponds to geologic patterns and structures of the study area. High amplitudes were associated with response from shallow intrusive basement rocks while low amplitudes were due to response from sources covered with thick sediments.

The First Vertical derivative helped in the delineation of geological structures B1, B2 and B3 as cringing surface features. The first Vertical derivatives also delineated lineaments F1, F2, F3, F4, F5, F6, F7, and F8. F1 and F8 are folds in yellow colour, F2, F3, F4 and F5 are associated with the iron ore mineralised region between Agbaja and Tajimi. The longest lineament F6 is a fault line running diagonally from SE-SW cutting across the river Niger. F7 is a minor lineament at the SE edge.

CET automatically delineated major and minor structures showing regions with dense and sparse structures, the NW and SW regions hosted major structures and lineaments favourable for mineralisation.

The Euler depth and structural map revealed the depth to magnetic bodies, depths of 27 and 1252 M were recorded as minimum and maximum depth to magnetic sources respectively.

The delineated lineaments trending NE-SW and E-W on 1VD map also coincide with regions delineated as K-Feldspar rich zone of Kogi state (Fatoye, 2018). The affected regions being part of the basement region of study area also represent the highly favoured zone of mineralisation.

The radiometric Concentration and Ratio maps helped in defining lithology boundaries and comparative abundance of the three radiogenic elements. The NW and SW regions which are typically basement in composition were seen to portray K dominance while NE and SE regions which are associated with sedimentary geology showed prominence of Th and U.

The K/Th ratio map was essential for delineating regions of hydrothermal alterations due to evidence of K enrichment at the expense of Th and quantitative occurrence of K/Th ratio value above known threshold of 0.2 %/ppm at designated areas in the NW and SW regions of study area. The regions around Latitude 8°00’ and 7°30’ within the NW and SW respectively were mapped on the K/Th ratio map with colour shades of pink to be the areas to have undergone K enrichment due to hydrothermal alteration. The regions of alterations are also Potential sites for gold mineralisation because gold deposits often occur in the hydrothermal altered zones rich in potassium (Ohioma *et al.,* 2017).

The ternary map revealed the western regions of the study area as dominated by potassium enriched feldspar. The NE regions hosting majorly iron stone gravel

The maximum value of geothermal gradient (66.69 °C/km) and Heat flow (166.74 mW/m^2) occur at the western edge of Lokoja where the Curie point depth has the least

value (8.69 kilometres). The heat flow ranging from 60 to 166 mW/m^2 exceeds the continental average value of 60 mW/m^2 which is indicative of anomalous values that are good source of explorable geothermal energy.

CHAPTER FIVE

5.0 CONCLUSION AND RECOMMENDATIONS

5.1 Conclusion

The interpretation of Aeromagnetic and Radiometric data of the confluence area of Kogi state gave insight to useful geological deductions. Analysis of the airborne geophysical data set provided structural and lithology details of the basement and sedimentary geologies construed in the study area. The western region of study area is generally an extraction of the most mineralised western region of Kogi state, it is also the basement region of study area where most of the mineralised features were delineated. Deductions from the 1VD map shows major Structures in form of magnetic lineaments that shows areas of mineralisation at Agbaja, Emu, Tajimi and Koton-karfe (Fatoye 2018). Ternary and K/Th ratio maps both revealed the western regions to be rich in K-Feldspar minerals and also host hydrothermally altered zones. The zones of alteration also corresponds to the areas delineated to host major magnetic lineaments of mineral potential trending NE-SW and E-W direction of study area. This makes the NW and SW regions of study area hosting major lineaments and zones of hydrothermal alterations the zone of mineralisation that could be target for exploration of iron ore and K-feldspar related minerals such as gemstones (Fatoye 2018). Essential minerals such as gold could also be a target for exploration in the western region of study area as potential gold deposits often occur in the hydrothermal altered zones rich in potassium (Ohioma *et al*. 2017). The sedimentary regions in the northern and southern ends were delineated to host majorly sediments in the form of sandstone, shale, limestone, mudstone, coal, clay and alluvium.

The point (6.625 E, 7.75 N) on the western edge of Lokoja and entire mid-portion of study area recorded heat flow exceeding 80 mW/m^2 with a high geothermal gradient and

relatively low Curie point depth which are suitable geothermal parameters for a good potential geothermal source

5.2 Recommendations

The results of this work is regional in nature due to the extent of the area covered, ground-truthing could be a means of determining the economic viability of the potentials.

.

REFERENCES

Adagunodo, T. A., Sunmonu, L. A. & Adeniji, A. A.(2015). An overview of magnetic method in mineral exploration *Journal of Global Ecology and Environment* 3(1): 13-28

Adetona, A. A., & Mallam, A. (2013). Estimating the thickness of sedimentation within lower Benue basin and upper Anambra basin, Nigeria, using both spectral depth determination and source parameter imaging. *ISRN Geophysics*, *2013*, 1-10. https://doi.org/10.1155/2013/124706

Adetona, A. A., & Mallam, A. (2013). Investigating the structures within the lower Benue and upper Anambra basins, Nigeria, using first vertical derivative, analytical signal and (CET) centre for exploration targeting plug-in. *Earth Sciences*, *2*(5), 104. https://doi.org/10.11648/j.earth.20130205.11

Adewumi, T., Salako, K. A., Adediran, S. O., Okwokwo, O. I., & Sanusi, Y. A. (2019). Curie point depth and heat flow analyses over part of Bida basin, north central Nigeria using Aeromagnetic data. *Journal of Earth Energy Engineering*, *8*(1), 1-11. https://doi.org/10.25299/jeee. 8(1). 22-88

Akanbi E. S., & Fakoya A. D. (2015). Regional magnetic field trend and depth to magnetic source determination from aeromagnetic data of Maijuju Area, North Central, Nigeria. *Physical Science International Journal 8(3): 1-13, 2015, Article no.PSIJ.21652*

Akanmu, Y. R. (1998): Paleoenvironments of the Lokoja Sandstone in the Lokoja - Koton-Karfi Area of Central Nigeria. A BSc Project Report.

Akinnubi T. D., & Adetona A. A. (2018) Investigating the geothermal potential within Benue State, central Nigeria from radiometric and high resolution aeromagnetic data. *Journal of Geology and Mining Research. pp*.(9)10

Allis, R.G. (1990) Geophysical anomalies over epithermal systems, *Journal of Geochemical Exploration*, 36, pp. 339-374,

Amenyoh, T., Wemegah, D. D., Menyeh, A., & Danuor, S. K. (2009). The use of landsat and aeromagnetic data in the interpretation of geological structures in the Nangodi Belt, University of Cape Coast

Bhattacharyya, B. K. & Leu, L. K. (1977) Spectral analysis of gravity and magnetic anomalies due to rectangular prismatic bodies, *Geophysics*, 42, 41–50.

Bhattacharyya, B., & Leu, L. K. (1975). Analysis of magnetic anomalies over Yellowstone National Park: mapping of Curie point isothermal surface for geothermal reconnaissance. *Journal of Geophysical Research, 80*(32), 4461-4465

Blackwell Scientific Publication, London; 1991. DS. Principles of Applied Geophysics, 3rd Edition. Chapman and Hall, New York, USA; 1978

Blakely RJ. (1995) *Potential theory in gravity and magnetic applications*. Cambridge University Press. New York, USA;

Blakely, R. J. (1988) Curie temperature isotherm analysis and tectonic implications of aeromagnetic data from Nevada, J. *Geophysics*. *Resistivity*. 93, 817–832.

Blatt, H., and Tracy, R.J. (1996) *Petrology - Igneous, Sedimentary, and Metamorphic* 2nd edition W.H. Freeman and Company, 529p.

Chinwuko A. I., Usman A. O., Onwuemesi A. G., Anakwuba E. K., Okonkwo C. C., & Ikumbur E. B. (2014).Interpretations of aeromagnetic data over lokoja and environs, Nigeria *International Journal of Advanced Geosciences*, 2 (2) (2014) 66-71

Clark, D. A. (1997). Magnetic properties of rocks and minerals. *AGSO Journal of Australian Geology and Geophysics*

Colin, R. (2005). Aeromagnetic Surveys, Principles, Practice and Interpretation.

Colin, R. (2010). Aeromagnetic Surveys, Principles, Practice and Interpretation.

Cordell, L. & Grauch, V.J.S. (1985) Mapping basement magnetization zones from aeromagnetic data in the San Juan basin, New Mexico. In: Hinze, W.J., Ed., The utility of regional gravity and magnetic anomaly maps, Society of Exploration Geophysicists,181-197. http://dx.doi.org/10.1190/1.0931830346.ch16

Dalan, R.A. 2006. A geophysical approach to buried site detection using down-hole susceptibility and soil magnetic techniques. *Archaeological Prospection.*

Debeglia, N. & Corpel, J. (1997). Automatic 3D Interpretation of Potential Field Data Using Analytic Signal Derivatives. *Geophysics*, 62, 87-96. https://doi.org/10.1190/1.1444149

Elawadi, E, Ammar, A, & Elsirafy, A. (2004), Mapping surface geology using airborne gammaray spectrometric survey data - A case study. Proceedings of SEGJ *international symposium. Nuclear Materials Authority of Egypt*, Airborne Exploration Dept.

Fatoye, F. B. (2018) Geology and Mineral Resources of Kogi State, Nigeria *International Journal of Multidisciplinary Sciences and Engineering*, 9(7), 1-13

Fugro Gravity and Magnetic Services, Houston, USA pp. 990–1002.

Geosoft Inc., (1996): Oasis Montaj Version 6.3 User Guide, Geosoft Incorporated, Toronto

Geosoft Inc., (2010): Oasis Montaj Version 6.3 User Guide, Geosoft Incorporated, Toronto

Graham, K.M. (2013): Geological and structural interpretation of part of the Buem Formation, Ghana, usingaero geophysical Data. Unpublished M.Sc. thesis, Kwame Nkrumah University of Science and Technology, Kumasi, Ghana.

Grant, F. S. (1985). Aeromagnetic, geology of an ore environment, Magnetite in igneous, sedimentary and metamorphic rocks. *An overview of Geoexploration.*

Gunn, P. J., Minty, B. R. S., & Milligan, P. (1997). The airborne gamma-ray spectrometric Response over arid australian terranes. *Exploration*, 97: pp. 733–740.

Hoover, D.B., Heran, W.D. and Hill, P.L. (1992). The Geophysical Expression of Selected Mineral Deposit Models. U.S. Geological Survey Open-File report 92–557, pp. 129

International Atomic Energy Agency (1990). The use of gamma rays data to define the natural radiation Environment, Vienna.

International Atomic Energy Agency (2003). Guidelines for radioelement mapping using gamma ray spectrometry data, Vienna.

ICRU (1994). Gamma ray Spectrometry in the Environment, ICRU Report 53. International Commission on Radiation Units And Measurements, Bethesda, USA

Ibe, S. O., & Nwokeabia, C. N. (2020). Application of airborne radiometric method in geologic mapping of malufashi area and environs, north western *Nigeria International Journal of Advanced Geosciences*, 8 (2) (2020) 179-185

Imrana, Dr.I.V Haruna (2017) Geology, Mineralogy And Geochemistry 0f Koton-Karfe Oolitic Iron Ore Deposit, Bida Basin. Kogi State, Nigeria *International Journal of Scientific & Technology Research* Volume 6

Kearey, P, Brooks, M, Hill I. (1991), *An Introduction to Geophysical Exploration* Second Edition. TJ international. pp. 2-160

Kearey, P, Brooks M, Hill I. (2002), *An Introduction to Geophysical Exploration* third Edition. TJ international. pp. 2-160

Kogi State Ministry of Solid Minerals Development, KSMSMD (2004). Guide to Investment Opportunities in the Solid Minerals Sector of Kogi State. 26 p.

Li, X. (2008). Magnetic reduction-to-the-pole at low latitudes. The Meter Reader, pages

Liu, S., & Mackey T. (1998). Using images in a geological interpretation of magnetic data. AGSO Research Newsletter 28.

Lu, R.S, Mariano J. & Willen D.E, (2003) Differential reduction of magnetic anomalies to the pole on a massively parallel computer. *Geophysics*, 68 (6): 1945-1951

Manu, J. (1993). Gold deposits of Birimian greenstone belts in Ghana: Hydrothermal. Alteration and Thermodynamics. Verlag Mainz, Wissenchaftsverlag, Aachen Herstellung: Fotodruck Mainz GmbH Susterfeldstr. 83. 52072 Aachen

Milligan, P., & Gunn, P. (1997). Enhancement and presentation of airborne geophysical data. *AGSO Journal of Australian Geology & Geophysics, 17*(2), 63-75.

Ministry of Mines and Steel Development (MMSD) (2010) Iron Ore Exploration Opportunities in Nigeria.

Minty, B. R. S. (1997). The fundamentals of airborne gamma-ray spectrometry. *AGSO Journal of Australian Geology and Geophysics.*

Nagata, T. (1961). Rock Magnetism. Maruzen Company. P 350.

Nigeria Geological Survey Agency, (2009) Geological map of Nigeria https://ngsa.gov.ng/geological-maps

Nigeria Geological Survey Agency, (2009) Airborne geophysical survey specifications https://ngsa.gov.ng/geological-maps

Nuri, D. M, Timur U. Z, Mumtaz H, & Naci, O. (2005). Curie Point Depth variations to infer thermal structure of the crust at the African-Eurasian convergence zone, SW Turkey. *Journal of Earth Planets Space,* 57(5):373-383.

Nwankwo L. I. & Abayomi J. S. (2017) Regional estimation of Curie-point depths and succeeding geothermal parameters from recently acquired high-resolution aeromagnetic data of the entire Bida Basin, north-central Nigeria *Geothermal energy science*., 5, 1–9, doi:10.5194/gtes

Nwankwo L. I, Olasehinde, P. I. & Akoshile C. O. (2008). Spectral analysis of aeromagnetic anomalies of the Northern Nupe Basin, West Central Nigeria, *Global Journal Of Pure And Applied Sciences*. 14(2), 1-8

Nwobodo A.N, Abangwu, U. J,Omeke, N.E (2018) Investigation of Magnetic Anomalies Of Lokoja And Dekina Areas, Lower Benue Trough Nigeria, Using High Resolution Aeromagnetic Data. *Journal of Applied Physics (IOSR-JAP) e-ISSN: 2278-4861.Volume 10, Issue 5 Ver. III), 39-47*

Nwofor, V. U., Opara, A. I., Echetama, H. N., Emberga, T. T, & Inyang G. E. (2018). Magnetic basement depth and structure over parts of bida basin, nigeria interpreted from 2-d spectral analysis and 3-d euler deconvolution. *Australian Journal of Basic and Applied Sciences* pages 1-9 DOI: 10.22587/ajbas.

Obaje N.G. (2009), Geology and Mineral Resources of Nigeria, Lecture Notes in Earth Sciences pp.218

Obiora D. N., John A. Y., Francisca N. O., Josiah U. C. & Andrew I. O. (2016). Interpretation of aeromagnetic data of idah area in north central nigeria using combined methods *Journal Geological Society of India,* 88, 98-106

Ohioma, J. O, Ezomo F., & Akinsunmade (2017). Delineation of hydrothermally altered zones that favour gold mineralization in isanlu area, Nigeria using aeroradiometric data, *International Annals of Science* ISSN: 2456-7132 Volume 2, Issue 1, pp. 20-27

Okubo, Y., Graff, R. G., Hansen, R. O., Ogawa, K., and Tsu, H. (1985) Curie point depths of the Island of Kyushu and surrounding areas, Geophysics, 53, 481–494.

Olasehinde, P. I., Adepitan. E. A. (2012). Analysis and interpretation of aeromagnetic anomaly map of Koton-Karfi (Sheet 227), North-Central, Nigeria. *Continental J. Earth Sciences* 7 (2): 26 – 31.

Ostrovskiy, E. A. (1975). Antagonism of radioactive elements in well rock alteration fields and its use in aerogamma spectrometric prospecting. *International Geological Review,* 17: pp. 461–8.

Plumlee, G. S., Smith, K. S., Ficklin, W. H., and Briggs, P. H. (1992). Geological and geochemical controls on the composition of mine drainages and natural drainages in mineralized areas. Proceedings, *7th International Water-Rock Interaction Conference*. Park City, Utah, July, 1992. pp. 419–422

Portnov, A. M. (1987). Specialization of Rocks toward Potassium and Thorium in Relation to Mineralization. International Geological Review, vol. 29, pp. 326–344. https://doi.org/10.1080/00206818709466149

Ramadass G., A. SubhashBabu, G. Udaya Laxmi (2013) Structural analysis of airborne radiometric data for identification of kimberlites in parts of Eastern Dharwar Craton *International Journal of Science and Research (IJSR)* Volume 4 Issue 4, www.ijsr.net

Reid, A.B., Allsop, J. M., Granser, H., Millet, A. J., & Somerton, I. W. (1990) Magnetic interpretation in three dimensions using Euler deconvolution: *Geophysics,* 55, p. 80-91.

Roest, W. R. & Pilkington, M. (1992). Identifying remanent magnetization effects in magnetic data. Geophysics, 58: pp. 653–659.

Ross, H. E., Blakely, R. J., and Zoback, M. D. (2006) Testing the use of aeromagnetic data for the determination of Curie depth in California, Geophysics, 71, L51–L59.

Salako K. A. (2014), Depth to basement determination using source parameter imaging (spi) of aeromagnetic data: An application to upper benue trough and Borno basin, Northeast, Nigeria. *Academic Research International* 5(3) 17-27

Schwarzer, T. F. and J. A. S. Adams, "Rock and soil discrimination by low altitude airborne gamma-ray spectrometry in Payne County, Oklahoma," *Economic Geology,* 1973, pp.1297–1312

Silva, A., Pires, A., Mccafferty, A., De Moraes , R., & Xia, H. (2003). Application of Airborne Geophysical Data to Mineral Exploration in the Uneven Exposed Terrains of the Rio Das Velhas Greenstone Belt. *Revista Brasileira de Geociências, 33,* 17-28.

Spector, A., & Grant, F. (1970). Statistical models for interpreting aeromagnetic data. *Geophysics, 35*(2), 293-302

Stacey, F. O. (1977) Physics of the Earth, JohnWiley and Sons, New York.

Tanaka, A. Y., Okubo, Y., and Matsubayashi, O. (1999) Curie point depth based on spectrum analysis of the magnetic anomaly data in East and Southeast Asia, *Tectonophysics*, 306, 461–470.

Telford, W. M., Geldart, L. P., and Sheriff, R. E. (1990*). Applied Geophysics*. Cambridge University Press, second edition.

Thomas, M. D., Walker, J. A., Keating, P., Shives, R., Kiss, F., & Goodfellow, W. D. 2000. Geophysical atlas of massive sulphide signatures, Bathurst mining camp, New Brunswick: Geological Survey of Canada Open File 3887. 105 p.

Thompson, D. T. (1982) "EULDPH" A new technique for making computer-assisted depth estimates from magnetic data: *Geophysics*, 47, 31-37.

Trifonova, P., Zhelev, Z., Petrova, T., & Bojadgieva, K. (2009) Curie point depth of Bulgarian territory inferred from geomagnetic observations and its correlation with regional thermal structure and seismicity, Tectonophysics, 473, 362–374.

Tselentis, G. A. (1991). An attempt to define curie depths in Greece from aeromagnetic and heat flow data. Pure and Applied Geophysics 136:87-101.

Whitham, K. (1960). Measurement of the geomagnetic elements. In Methods and techniques in Geophysics 1, S. K. Runcorn

Wilford, J. R., Bierwirth, P. N., and Craig, M. A. (1997). Application of Airborne Gammaray Spectrometry in Soil/Regolith Mapping and Applied Geomorphology. AGSO *Journal of Australian Geology and Geophysics*, 17(2):201-216

APPENDIXES: GRAPH OF ENERGY SPECTRUM VERSUS WAVE NUMBER FOR SEECTION 1 - 8

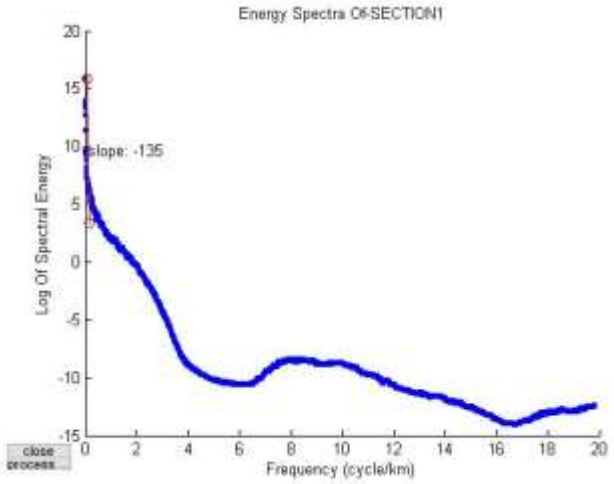

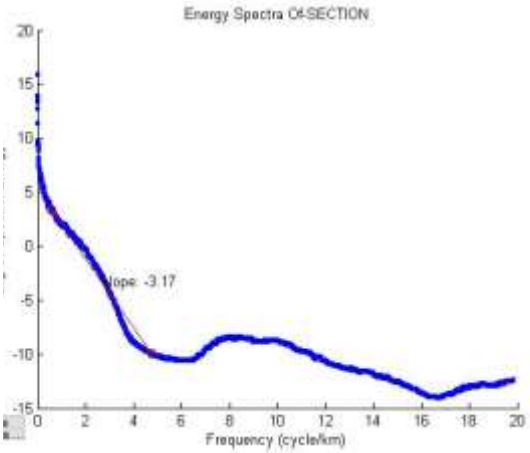

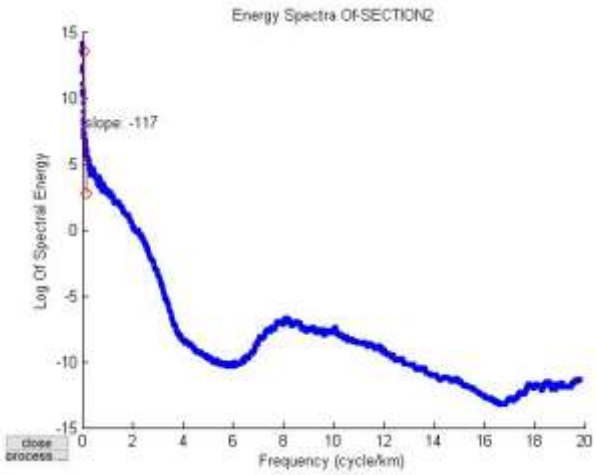

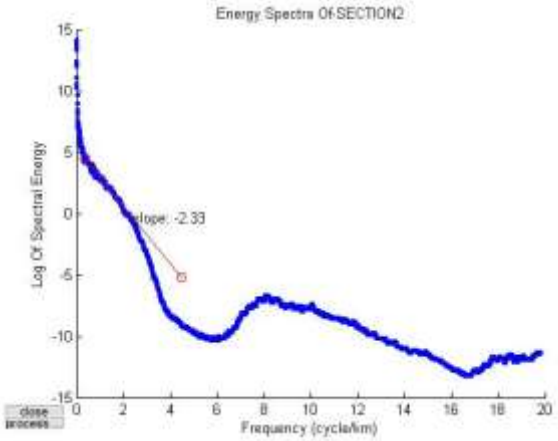

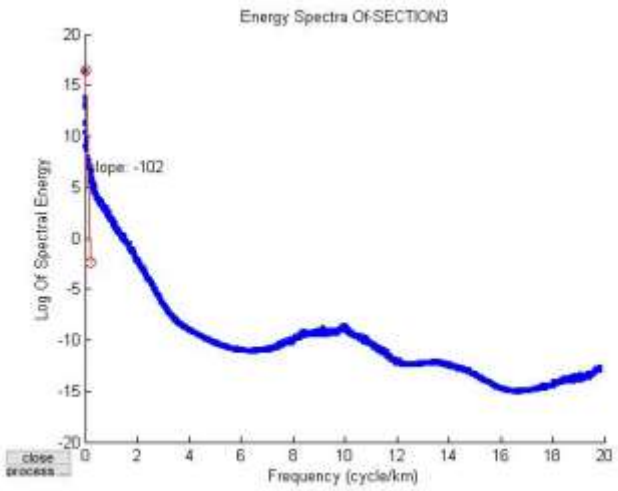
Energy Spectra Of-SECTION3
Log Of Spectral Energy
Slope: -102
Frequency (cycle/km)
close process

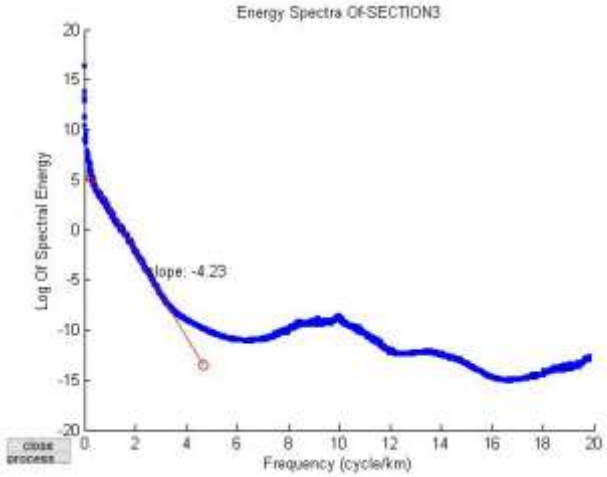
Energy Spectra Of-SECTION3
Log Of Spectral Energy
Slope: -4.23
Frequency (cycle/km)
close process

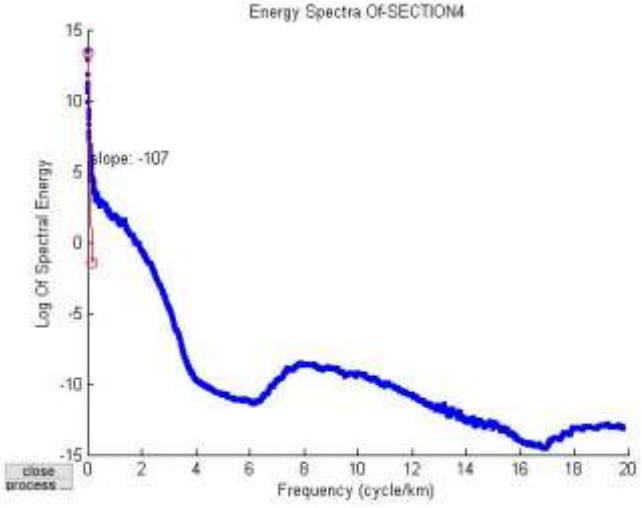
Energy Spectra Of-SECTION4
Log Of Spectral Energy
Slope: -107
Frequency (cycle/km)
close process

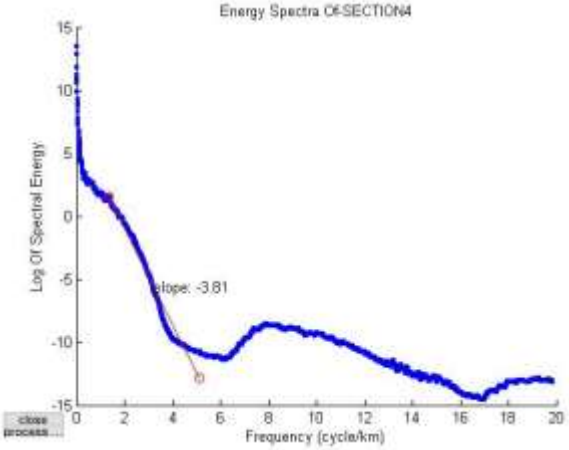
Energy Spectra Of-SECTION4
Log Of Spectral Energy
Slope: -3.81
Frequency (cycle/km)
close process

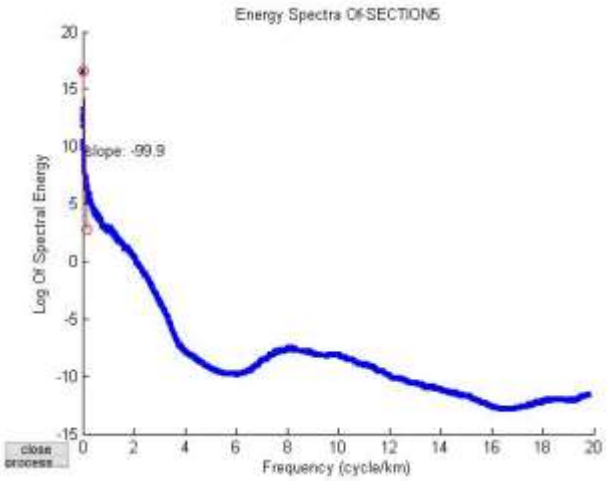
Energy Spectra Of-SECTION5
Log Of Spectral Energy
Slope: -99.9
Frequency (cycle/km)
close process

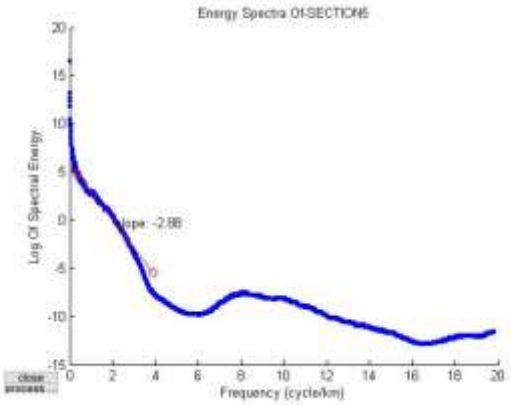
Energy Spectra Of-SECTION5
Log Of Spectral Energy
Slope: -2.88
Frequency (cycle/km)
close process

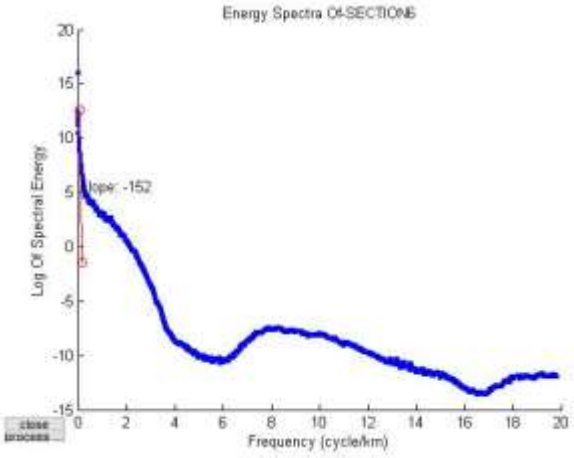
Energy Spectra Of-SECTION5
Log Of Spectral Energy
Slope: -152
Frequency (cycle/km)
close process

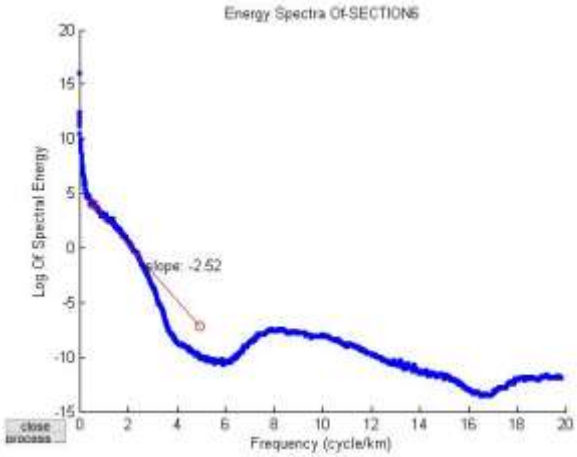
Energy Spectra Of-SECTION5
Log Of Spectral Energy
Slope: -2.52
Frequency (cycle/km)
close process

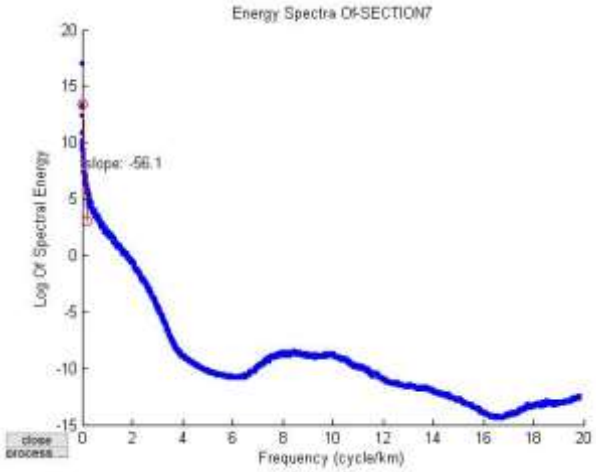
Energy Spectra Of-SECTION7
slope: -56.1
Log Of Spectral Energy
Frequency (cycle/km)
close process

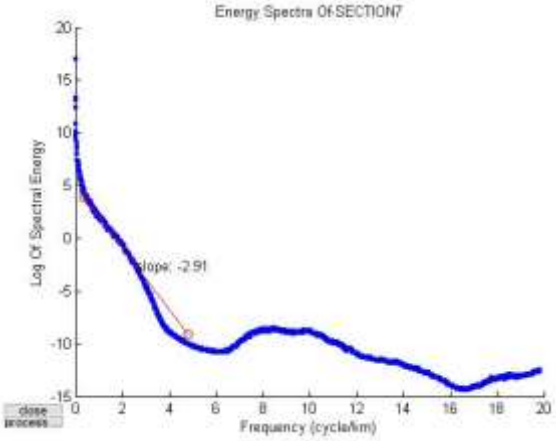
Energy Spectra Of-SECTION7
slope: -2.91
Log Of Spectral Energy
Frequency (cycle/km)
close process

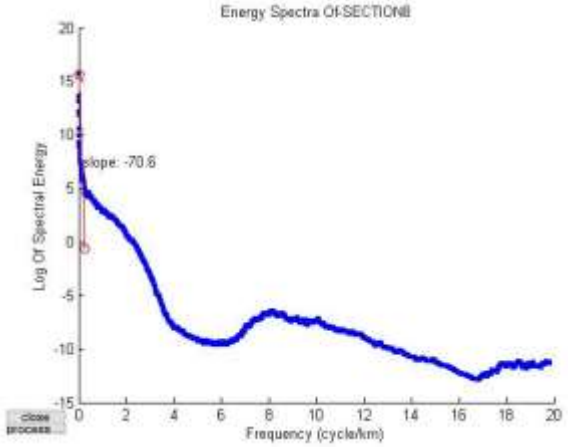
Energy Spectra Of-SECTION8
slope: -70.6
Log Of Spectral Energy
Frequency (cycle/km)
close process

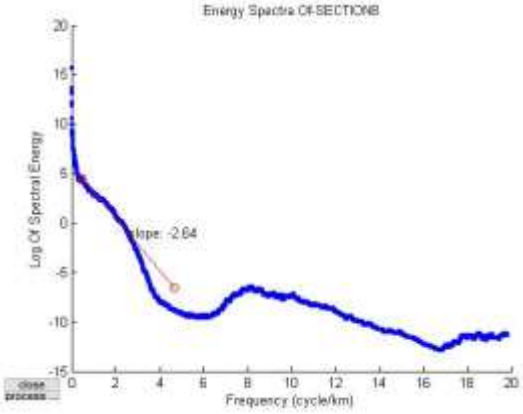
Energy Spectra Of-SECTION8
slope: -2.64
Log Of Spectral Energy
Frequency (cycle/km)
close process